APPLIED SCIENCES AND ENGINEERING

Injectable, self-healing hydrogel adhesives with firm tissue adhesion and on-demand biodegradation for sutureless wound closure

Hui Ren[1,2]†, Zhen Zhang[1]†, Xueliang Cheng[3], Zheng Zou[1,2], Xuesi Chen[1,2], Chaoliang He[1,2]*

Tissue adhesives have garnered extensive interest as alternatives and supplements to sutures, whereas major challenges still remain, including weak tissue adhesion, inadequate biocompatibility, and uncontrolled biodegradation. Here, injectable and biocompatible hydrogel adhesives are developed via catalyst-free *o*-phthalaldehyde/amine (hydrazide) cross-linking reaction. The hydrogels demonstrate rapid and firm adhesion to various tissues, and an *o*-phthalaldehyde–mediated tissue adhesion mechanism is established. The hydrogel adhesives show controlled degradation profiles of 6 to 22 weeks in vivo through the incorporation of disulfide bonds into hydrogel network. In liver and blood vessel injury, the hydrogels effectively seal the incisions and rapidly stop bleeding. In rat and rabbit models of full-thickness skin incision, the hydrogel adhesives quickly close the incisions and accelerate wound healing, which exhibit efficacies superior to those of commercially available fibrin glue and cyanoacrylate glue. Thus, the hydrogel adhesives show great potential for sutureless wound closure, hemostasis sealing, and prevention of leakage in surgical applications.

INTRODUCTION

Every year, millions of individuals are inflicted with various types of wounds, including those attributed to accidental trauma and surgical incisions. After tissue injury, massive bleeding and wound infections are major causes of mortality (*1*, *2*). Although sutures and staples are currently the most common approaches used for wound closure in clinical treatments, the time-consuming operations and demanding technical requirements involved render them unsuitable for many emergency situations, such as sudden natural disasters and war. Moreover, they are usually associated with secondary tissue damage and leakage of fluid or air, particularly in the fragile viscera (*3*–*5*). In recent years, adhesives have garnered substantial interest as substitutes or complements to sutures and staples (*6*, *7*).

Tissue adhesives have been used for wound closure, hemostasis, prevention of anastomotic leakage, and consequent acceleration of wound healing (*8*–*11*). However, commercially available adhesives still fail to meet clinical requirements owing to drawbacks such as weak tissue adhesion, toxic components, and uncontrollable biodegradation. For instance, fibrin glues have been approved by the U.S. Food and Drug Administration (FDA) for closure and hemostasis of various types of wounds. Nevertheless, they show weak adhesion to tissues (5 to 10 kPa) and pose a risk of diseases with blood-borne viruses (*12*). Cyanoacrylate glues demonstrate relatively high adhesion strength and have been approved for the closure of skin wounds; however, the toxic cyanoacrylate monomers and degradation products of their polymers limit their internal clinical applications (*13*, *14*).

In recent years, various adhesion mechanisms have been investigated to develop next-generation tissue adhesives with superior performance. The mechanisms underlying tissue adhesion typically include the formation of covalent conjugation between adhesives and the tissue surface (*11*), as well as physical interactions, such as hydrogen bonding, electrostatic interactions, and π-π interactions (*15*–*17*). To date, tissue adhesion mechanisms that depend on covalent conjugation have been examined extensively. Typically, covalent bonding between tissues and adhesives is realized via reactions between active groups (amine or thiol group) on the tissue surface and reactive groups, such as *N*-hydroxysuccinimide (NHS) esters (*18*–*22*), aldehydes (*23*–*25*), and polyphenols (*26*–*31*) in adhesives. Nevertheless, these cross-linking approaches still have considerable drawbacks. For instance, owing to the hydrolytic instability of NHS ester, the adhesion performance may be compromised after rehydration and long-term storage of the NHS ester (*32*). Adhesives whose mechanisms are based on aldehyde/amine condensation commonly show relatively low adhesion strength because of the reversible nature of Schiff base bonds (*25*). In addition, tissue adhesion has been developed on the basis of biomimetic polyphenol groups, especially catechol and pyrogallol. However, oxidants are typically required for the oxidation of catechol to quinone to achieve firm adhesion, which may compromise the biocompatibility of the materials (*10*).

In addition, the biodegradation of adhesives also plays a crucial role in wound healing (*33*–*35*). In particular, the controlled degradation of tissue adhesives has advantages in practical applications of wound closure, such as controlled absorption or on-demand detachment of adhesives during tissue regeneration. Therefore, for tissue adhesives, ensuring an ideal adhesion mechanism, biocompatibility, and biodegradability remains a major challenge for their practical applications and clinical translation.

In our recent study, we discovered that the condensation reaction between *o*-phthalaldehyde (OPA) and *N*-nucleophiles (amine, hydrazide, and aminooxy groups) can be used for the development of a catalyst-free, fast, and biocompatible cross-linking strategy for

[1]CAS Key Laboratory of Polymer Ecomaterials, Changchun Institute of Applied Chemistry, Chinese Academy of Sciences, Changchun 130022, China. [2]School of Applied Chemistry and Engineering, University of Science and Technology of China, Hefei, Anhui 230026, China. [3]Department of Spinal Surgery, The Second Hospital of Jilin University, Changchun, Jilin 130014, China.
*Corresponding author. Email: clhe@ciac.ac.cn
†These authors contributed equally to this work.

hydrogel formation (*36*). During the cross-linking process, the reaction between OPA and amine (or hydrazide) proceeds spontaneously and chemoselectively under physiological conditions, resulting in the formation of stable phthalimidine (or reversible hydrazone) linkages. Nevertheless, the feasibility of using the OPA/*N*-nucleophile condensation reaction to develop tissue adhesives and properties of adhesion between OPA-functionalized materials and tissues have not yet been elucidated.

In this study, the OPA/*N*-nucleophile condensation reaction was used to construct hydrogel adhesives using hydrazide-modified hyaluronic acid (HA) and OPA-terminated four-armed poly(ethylene glycol) (4aPEG-OPA) as building blocks (Fig. 1). The OPA/hydrazide cross-linked hydrogels were designed owing to the dynamic nature of hydrazone linkages, which may impart self-healing properties to the bulk system. In addition, firm adhesion of the hydrogel to tissues can be realized through the spontaneous coupling of OPA with the amine groups present in tissues, typically in the proteins of the extracellular matrix, via the formation of stable phthalimidine bonds (*37*, *38*). We studied the physicochemical properties of the hydrogels, including gelation time, mechanical properties, and in vitro biocompatibility, and evaluated the ex vivo tissue adhesion properties of the hydrogels on various tissues. We also investigated the degradation of the hydrogels by implantation into the subcutaneous layer, which can be realized on-demand via the incorporation of disulfide bonds into the cross-linking network. Moreover, we demonstrated the potential application of hydrogel adhesives for in vivo hemostasis in animal models of liver and blood vessel injury and further systematically evaluated the wound closure performance of the hydrogels in rat and rabbit models of full-thickness skin incision.

RESULTS

Synthesis and characterization of hydrogel

HA is an essential component of the extracellular matrix and has been used in clinical applications for decades (*39*–*42*). We first synthesized the precursor polymer, adipic acid hydrazide–modified HA (HA-ADH), according to a previously reported method (fig. S1) (*43*). The degree of substitution was 11.8%, as observed by comparing the integral of the methylene proton of ADH at 1.53 parts per million (ppm) to the methyl proton in *N*-acetylglucosamine of the HA backbone at 1.89 ppm in ^{1}H nuclear magnetic resonance (NMR) spectrum (fig. S2). 4aPEG-OPA was prepared by introducing OPA groups to the terminals of 4aPEG (M_n = 10 kDa) as a cross-linker, according to our previously reported procedure (*36*). On the basis of the ^{1}H NMR spectrum, the degree of modification of OPA on the terminals of 4aPEG was 75% (fig. S3).

HA-ADH/4aPEG-OPA (denoted as HA-PEG) hydrogels were formed by simply mixing HA-ADH with 4aPEG-OPA at a mass ratio of 1:1 in phosphate-buffered saline (PBS) under physiological conditions without the involvement of any catalyst. Time-dependent ^{1}H NMR analysis indicated that the reaction between OPA groups of 4aPEG-OPA and hydrazide groups of HA-ADH resulted in the formation of isoindole bis(hemiaminal) (IBHA) heterocyclic intermediate, which further underwent dehydration to form the hydrazone (Fig. 2A) (*44*). As the residual aldehyde group could participate in another nucleophilic attack, the resultant hydrazone formed from OPA and hydrazide could further undergo an intramolecular cyclization to yield a cyclic product. To provide insights into the cross-linking process, the mechanism of the reaction between OPA and hydrazide was investigated by density functional theory (DFT) calculations using model molecules (Fig. 2B). For the hydrazone formation from benzaldehyde and acethydrazide, the dehydration of the hemiaminal intermediate is rate determining, corresponding to the highest barrier of 31.98 kcal/mol along the path (fig. S4). By contrast, OPA reacted with acethydrazide to yield the IBHA intermediate. The IBHA intermediate further dehydrates to form the hydrazone, and the energy barrier of this step was 22.66 kcal/mol, which was much lower than that of benzaldehyde counterpart. This result suggested that OPA could be used as a highly reactive cross-linking group for fast formation of hydrogel.

Fast gelation is a basic requirement of hydrogel adhesives. The gelation time of the HA-PEG hydrogel, which indicates the time required for the change from liquid to free-standing hydrogel, was evaluated using the vial inversion method at pH 7.4 and 37°C (Fig. 2C). Owing to the fast formation of the IBHA intermediate between OPA and hydrazide (*36*), the gelation time of the HA-PEG hydrogel was significantly shorter than that of its widely used benzaldehyde-based counterparts. As shown in Fig. 2D, when the HA-ADH/4aPEG-OPA mass ratio was fixed at 1:1, the gelation time of OPA/hydrazide cross-linked HA-PEG hydrogels was 2.0 ± 0.1, 1.5 ± 0.2, and 1.3 ± 0.1 min for polymer concentrations of 4, 7, and 10% (w/v), respectively. In contrast, the gelation time of HA-ADH/benzaldehyde-terminated 4aPEG (4aPEG-PhCHO) counterparts were 231 ± 6, 89 ± 1, and 49 ± 1 min under the same conditions. Cryo–scanning electron microscopy (cryo-SEM) images showed the formation of a porous structure in HA-PEG hydrogels (fig. S5A), which is beneficial for the transportation of active molecules and cells.

Subsequently, the time-sweep rheological test was performed at 37°C to monitor the evolution of storage modulus (G') and loss modulus (G'') during the cross-linking process. The G' values of 4 to 10% (w/v) HA-PEG hydrogels rapidly increased over G'' values within 0.5 min and then reached a plateau within 20 min (Fig. 2E), suggesting a dominant elastic behavior of the system and rapid hydrogel formation (*45*). Comparatively, the G' values of the benzaldehyde/hydrazide cross-linked HA-ADH/4aPEG-PhCHO hydrogels showed no apparent increase until 20 min (fig. S5B). The G' value of the HA-PEG hydrogel could be tuned by varying the polymer concentration. As the polymer concentration increased from 4 to 10% (w/v), the G' values of the hydrogel at the plateau markedly increased from 4.7 to 14.8 kPa, likely attributed to the increase in cross-linking density (*46*). Besides, the frequency sweep rheological test showed that the G' of 7% (w/v) HA-PEG hydrogel was almost constant in the range of 1 to 100 Hz (fig. S5C). In the strain sweep rheological test, the hydrogel exhibited linear viscoelasticity with strains ranging from 1 to 100%, whereas the G' of the hydrogel dropped rapidly at strains beyond 100% (fig. S5D). Owing to the reversible nature of hydrazone linkages formed between OPA and hydrazide (*47*), the hydrogel exhibited self-healing properties. By cutting the hydrogel into two pieces and placing them in contact with each other, the two pieces healed into a piece of hydrogel after 20 min, which could maintain its integrity under gravity (Fig. 2F). The self-healing properties of the hydrogels at polymer concentrations of 4, 7, and 10% (w/v) were evaluated by step-strain rheological tests between a strain of 1 and 500% at time intervals of 1, 2, 3, and 5 min. When the HA-PEG hydrogels were subjected to a strain of 500%, an inversion of G'

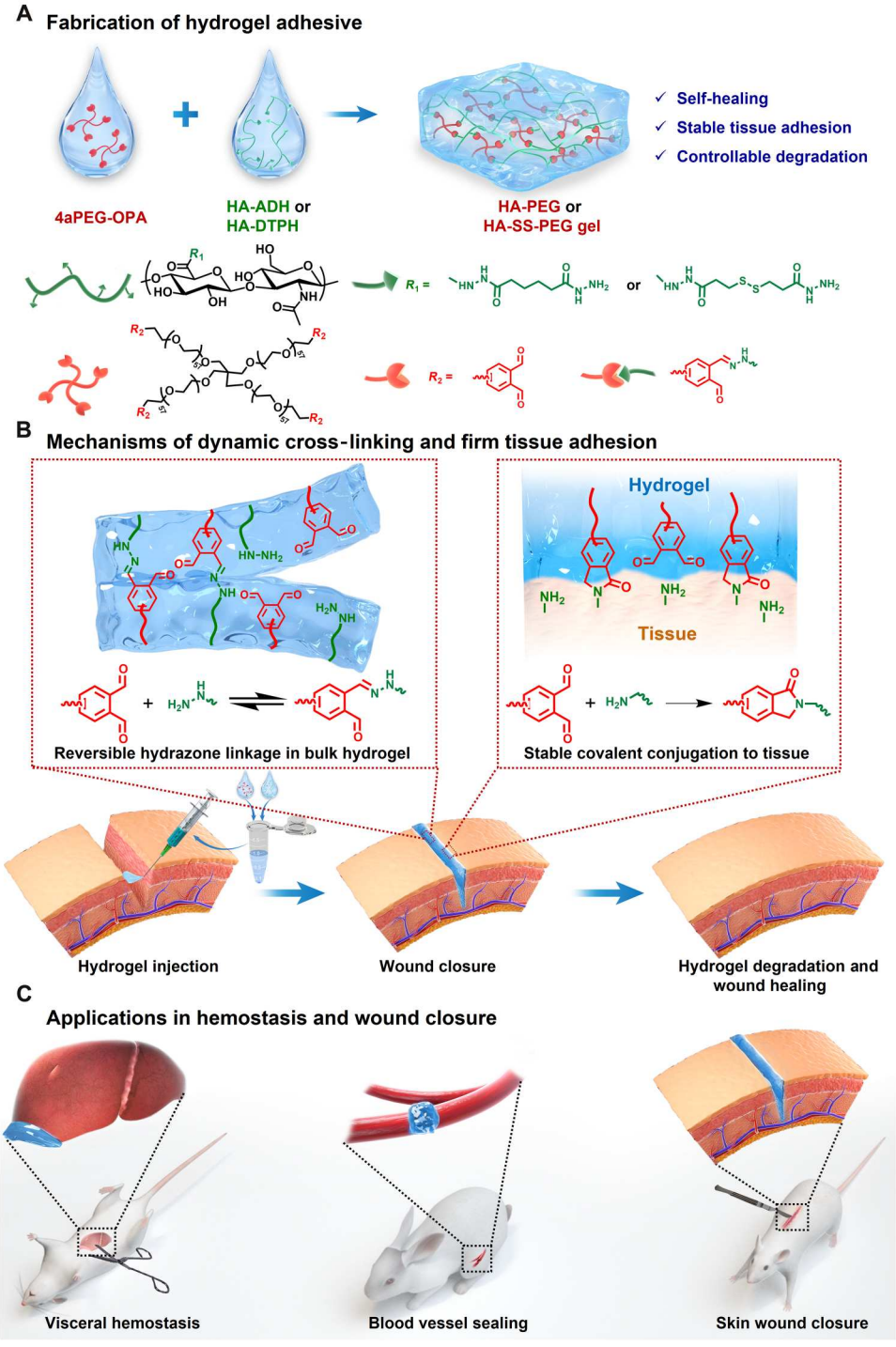

Fig. 1. Schematic illustration of the fabrication, cross-linking/adhesion mechanisms, and applications of hydrogel adhesive. (**A**) Fabrication of hydrogel adhesives was performed by mixing HA-ADH or HA-DTPH with 4aPEG-OPA. (**B**) Mechanisms of dynamic cross-linking in bulk hydrogel and firm hydrogel-tissue adhesion, respectively. (**C**) Application of hydrogel adhesives in hemostasis sealing and skin wound closure.

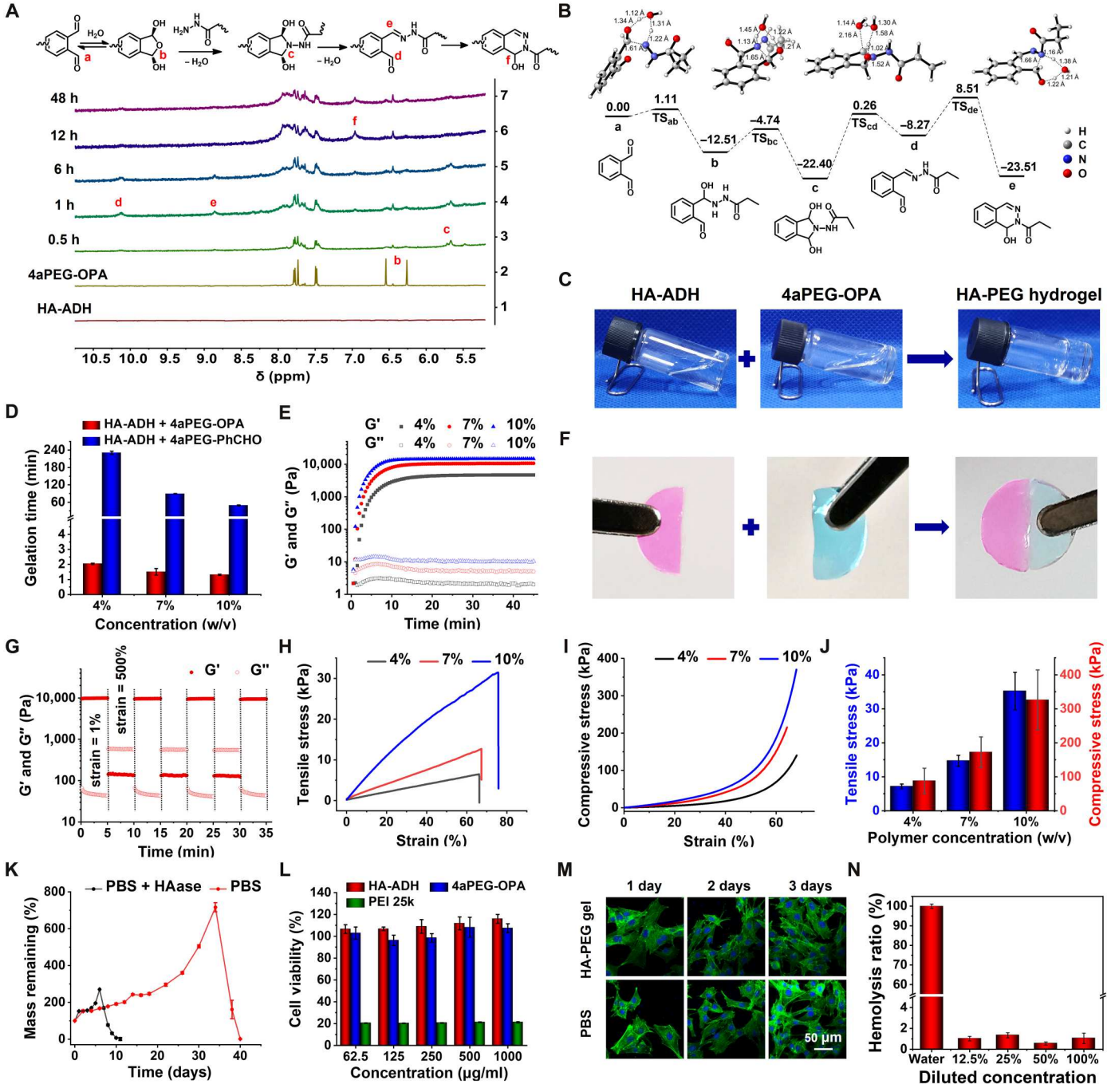

Fig. 2. Characterization of HA-PEG hydrogel. (**A**) Time-dependent ^{1}H NMR analysis of mixture of HA-ADH and 4aPEG-OPA in D_2O. (**B**) Energy profile calculated for hydrazone formation from OPA and acethydrazide [B3LYP/6-31+G(d,p), kcal/mol]. (**C**) Images of the formation of 7% (w/v) HA-PEG hydrogel. (**D**) Gelation time of HA-PEG hydrogels at different polymer concentrations at 37°C (mean ± SD, $n = 3$). (**E**) Storage modulus (G') and loss modulus (G'') of HA-PEG hydrogels in the time sweep test. (**F**) Images of self-healing behavior of 7% (w/v) HA-PEG hydrogel. The divided hydrogel pieces healed into a piece of hydrogel after contacting at 37°C for 20 min. (**G**) Step-strain measurement of 7% (w/v) HA-PEG hydrogel at a time interval of 5 min. (**H**) Representative tensile stress-strain curves of HA-PEG hydrogels at different polymer concentrations 6 hours after hydrogel formation at 25°C. (**I**) Representative compressive stress-strain curves of HA-PEG hydrogels at different polymer concentrations 6 hours after hydrogel formation at 25°C. (**J**) Quantitative data of tensile stress (mean ± SD, $n = 5$) and compressive stress (mean ± SD, $n \geq 4$) of different hydrogels. (**K**) Degradation profile of 7% (w/v) HA-PEG hydrogels in blank PBS and PBS with hyaluronidase (10 U/ml) at 37°C (mean ± SD, $n = 3$). (**L**) Viability of NIH 3T3 cells treated with different polymer solutions for 24 hours; polyethyleneimine 25k (PEI 25k) was used as a positive control (mean ± SD, $n = 5$). (**M**) Confocal images of NIH 3T3 cells co-cultured with 7% (w/v) HA-PEG hydrogel. (**N**) Hemolytic ratio of 7% (w/v) HA-PEG hydrogel extracts at different concentrations (mean ± SD, $n = 5$).

and G'' was observed, indicating that the viscous behavior became dominant owing to the breakage of cross-links at high strain (Fig. 2G and figs. S6 to S8) (*45*). At time intervals of 2, 3, and 5 min, the 4, 7, and 10% (w/v) hydrogels showed an almost complete recovery of both G' and G'' values after the strain was decreased to 1%. This recovery could be reproduced over three cycles. In contrast, at a time interval of 1 min, the step-strain rheological test showed a delay of recovery of G' values after the strain was decreased to 1%. The self-healing properties of the hydrogel were ascribed to the reversible nature of hydrazone linkages formed between OPA and hydrazide (*47*). It is beneficial for improving the durability and reliability of hydrogel adhesives by recovering their mechanical strength after damage (*48*).

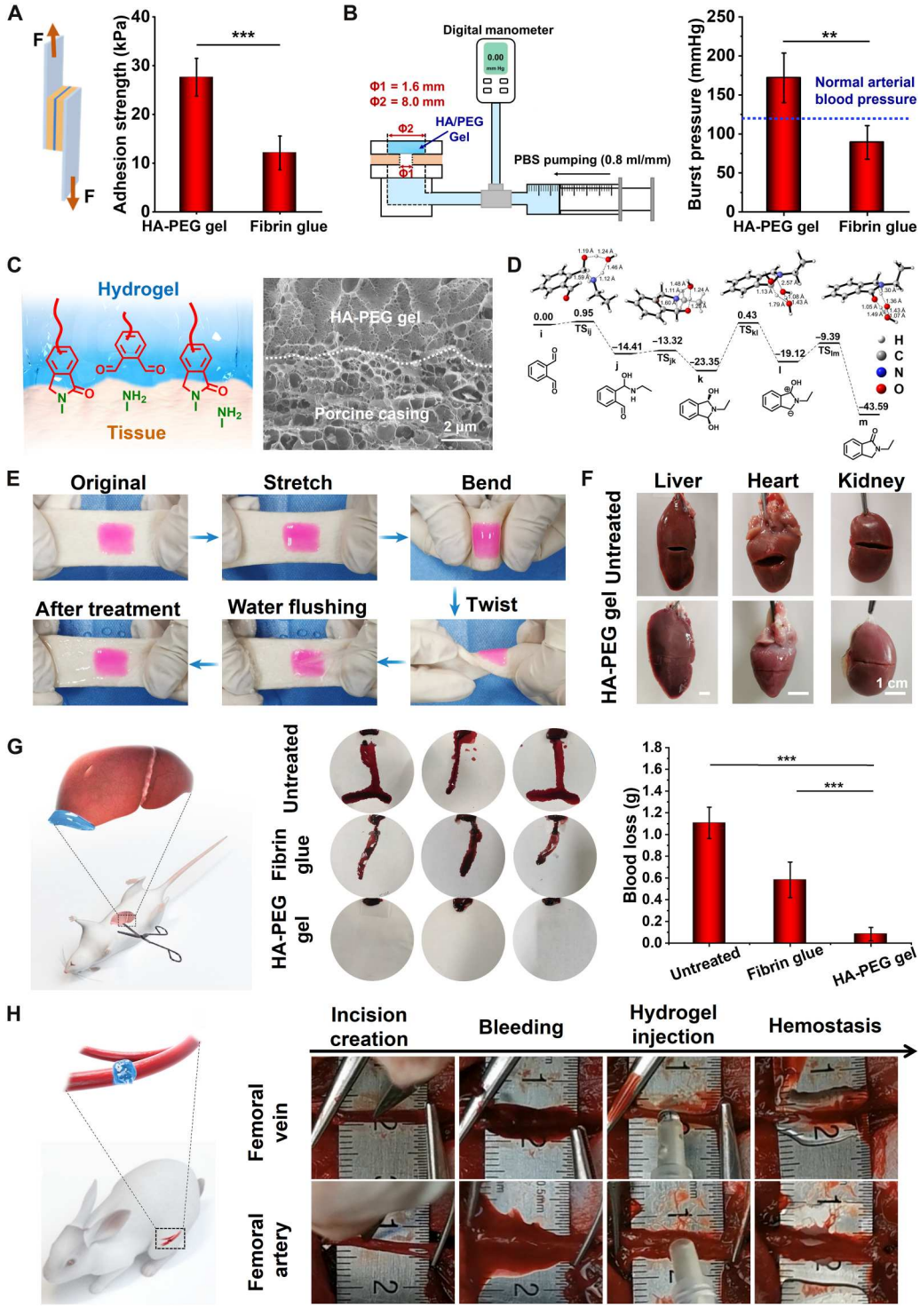

Fig. 3. Tissue adhesion properties and hemostatic performance of HA-PEG hydrogel. (**A**) Adhesion strength of 7% (w/v) HA-PEG hydrogel or fibrin glues to porcine skin at 37°C (mean ± SD, $n = 5$). (**B**) Burst pressure of porcine sausage casings sealed by 7% (w/v) HA-PEG hydrogel and fibrin glues recorded at 10 min after sealing (mean ± SD, $n = 5$). (**C**) Cryo-SEM images of the interface between porcine casing and 7% (w/v) HA-PEG hydrogel. (**D**) Energy profile calculated for the reaction between OPA and ethylamine [B3LYP/6-31+G(d,p), kcal/mol]. (**E**) Photographs of 7% (w/v) HA-PEG hydrogel adhered to porcine skin following stretching, bending, twisting, and flushing with water. (**F**) Photographs of ex vivo tissue adhesion and incision closure performance of 7% (w/v) HA-PEG hydrogel in the liver, heart, and kidney of a rabbit model. (**G**) Hemostatic effect of 7% (w/v) HA-PEG hydrogel on the rat liver in massive bleeding models. Schematic illustration, photographs, and blood loss showing liver bleeding of SD rats treated with fibrin glues or HA-PEG hydrogel (mean ± SD, $n = 5$). (**H**) Schematic illustration and photographs showing hemostatic sealing effects of 7% (w/v) HA-PEG hydrogel in rabbit femoral vein and artery incision models. Statistical significance was analyzed by independent sample *t* test for (A) and (B) and one-way ANOVA with the Tukey post hoc test for (G) (**$P < 0.01$ and ***$P < 0.001$).

We further evaluated the compressive and tensile strengths of HA-PEG hydrogels using a universal testing machine. As the polymer concentration increased from 4 to 10% (w/v), the compressive and tensile strengths of the hydrogel increased from 87.9 ± 37.3 kPa to 326.4 ± 87.8 kPa and 7.1 ± 0.7 kPa to 35.2 ± 5.5 kPa, respectively (Fig. 2, H to J, and fig. S9). These results collectively demonstrate that the mechanical properties of the hydrogel could be adjusted by varying the polymer concentration.

The biodegradation of adhesives plays a key role in wound healing and tissue regeneration. To investigate in vitro degradation of the HA-PEG hydrogel, we incubated 7% (w/v) hydrogels in blank PBS and PBS with hyaluronidase (10 U/ml). As shown in Fig. 2K, the hydrogels incubated in blank PBS swelled and then completely degraded in 40 days owing to a gradual cleavage of hydrazone linkages. The degradation rate of the hydrogel could be accelerated by adding hyaluronidase to the medium, which was attributed to the breakage of the HA backbone. The hydrogels were degraded within 11 days in the presence of hyaluronidase (10 U/ml). To investigate the influence of polymer concentration on hydrogel degradation, we evaluated the degradation behaviors of 4 and 10% (w/v) HA-PEG hydrogels in PBS containing hyaluronidase (10 U/ml). The hydrogels with 4 and 10% (w/v) polymer concentrations were degraded in 8 and 15 days, respectively (fig. S10). Overall, an increase of the polymer concentration from 4 to 10% (w/v) could prolong the time required for hydrogel degradation.

Good biocompatibility of both the polymer precursor solution and the resultant hydrogel is a basic requirement for biomedical applications, including the development of tissue adhesives. The cytocompatibility of the precursor polymers, HA-ADH and 4aPEG-OPA, against fibroblast NIH 3T3 cells was evaluated using the Cell Counting Kit-8 (CCK-8) assay at concentrations ranging from 0.0625 to 1 mg/ml for 24 hours. As shown in Fig. 2L, cell viability was more than 90%, suggesting no detectable cytotoxic effects of HA-ADH and 4aPEG-OPA. Subsequently, the HA-PEG hydrogel formed by mixing the two polymers was cocultured with NIH 3T3 fibroblasts for 3 days, and the cell viability was equivalent to that of the PBS group (Fig. 2M and fig. S11). In addition, the cells were mixed with precursor solutions and encapsulated in the hydrogel after cross-linking. Live-dead cell staining demonstrated a high viability of cells inside the hydrogel (fig. S11). The hemocompatibility of the hydrogels was further evaluated using hemolysis tests. As presented in Fig. 2N and fig. S12, the supernatant incubated with the hydrogel extract showed a light-yellow color, similar to that of saline. Quantitative analysis showed that the hemolysis rate of the hydrogel extract was less than 5%, indicating a good hemocompatibility of the hydrogel. These results confirmed that the HA-PEG hydrogel showed good biocompatibility in vitro.

Tissue adhesion properties and hemostatic performance of the HA-PEG hydrogel

To determine the tissue adhesion properties of the HA-PEG hydrogel, the hydrogel was sandwiched between two pieces of porcine skin, and the adhesion strength was measured using a lap shear test (Fig. 3A). The hydrogels with polymer concentrations of 4, 7, and 10% (w/v) showed adhesion strengths of 18.0 ± 1.8 kPa, 27.6 ± 3.9 kPa, and 30.3 ± 4.6 kPa, respectively (fig. S13). By increasing the polymer concentration from 4 to 7% (w/v), the adhesion strength of hydrogels was obviously increased from 18.0 ± 1.8 kPa to 27.6 ± 3.9 kPa. However, a further increase of concentration to 10% (w/v) only resulted in a slight increase of adhesion strength to 30.3 ± 4.6 kPa. In addition, the adhesion strength of the 7% (w/v) OPA/hydrazide cross-linked HA-PEG hydrogel (27.6 ± 3.9 kPa) was significantly higher than those of a commercially available fibrin glue (12.1 ± 3.5 kPa) and 7% (w/v) benzaldehyde/hydrazide cross-linked HA-ADH/4aPEG-PhCHO hydrogel counterpart (0.9 ± 0.8 kPa) (Fig. 3A and fig. S13). Moreover, a burst pressure test was carried out by applying the hydrogel onto the hole (~1.6 mm) of a casing to evaluate the ability of the HA-PEG hydrogel to prevent liquid leakage or bleeding when used as a tissue adhesive (Fig. 3B). It was found that the burst pressures were 67.8 ± 20.5 mmHg, 171.9 ± 31.8 mmHg, and 296.4 ± 47.0 mmHg for the hydrogels with polymer concentrations of 4, 7, and 10% (w/v), respectively (fig. S14). The burst pressures for the 7 and 10% (w/v) hydrogels were both significantly higher than those of the fibrin glue (89.1 ± 21.6 mmHg) and normal arterial blood pressure in humans (Fig. 3B) (*23*, *49*). Considering the appropriate adhesion strength and degradation behavior, a concentration of 7% (w/v) was selected for the HA-PEG hydrogel in subsequent experiments.

The interface between tissue and material was investigated by using cryo-SEM. As shown in Fig. 3C, a tight interface was formed between the porcine casing and the 7% (w/v) HA-PEG hydrogel. The robust adhesion of the hydrogel to various tissues can be attributed to the formation of stable phthalimidine linkages between the hydrogel and tissues (*37*, *38*). DFT calculation revealed that OPA reacted with primary amine to yield an IBHA intermediate, which then underwent dehydration and transformed into a phthalimidine product by tautomerization (Fig. 3D) (*50*, *51*). This reaction is strongly exoenergetic with an ΔE of 43.59 kcal/mol, suggesting the stability of phthalimidine linkage. In addition, the dynamic cross-linking networks based on hydrazone bonds provide the bulk hydrogel with the capability of energy dissipation. When a stress was applied, the cleavage of reversible hydrazone linkages and resulting dissipation of energy prevented the failure of adhesion at the adhesive-tissue interface. Cyclic compressive test was performed to validate the capability of energy dissipation of the HA-PEG hydrogel (fig. S15). The hysteresis loops of stress-strain curves suggested energy dissipation of the hydrogel, which was attributed to the cleavage of reversible hydrazone bonds in the hydrogel network.

To further demonstrate the tissue adhesion of the hydrogel, 7% (w/v) HA-PEG hydrogel was applied to various tissues ex vivo. The hydrogel showed strong adhesion to porcine skin without detachment after stretching, bending, twisting, or flushing with water (Fig. 3E). Besides, the hydrogel could adhere tightly to various tissues, including the liver, heart, and kidney, and achieve firm incision closure (Fig. 3F).

Excessive bleeding is a major cause of death during surgery and after trauma. Therefore, it is important to quickly seal the wounds and achieve hemostasis (*49*, *52*–*55*). We performed in vitro blood clotting experiments to explore the potential effect of 7% (w/v) HA-PEG hydrogel on promoting blood clotting (*56*). Blood clotting was observed at 0.4 ± 0.1 min and 1.1 ± 0.5 min for HA-PEG hydrogel and fibrin glue groups, respectively, much faster than the control group with a blood clotting time of 6.9 ± 1.4 min (fig. S16). It has been reported that the aggregation of platelets and red blood cells facilitated the formation of a hemostasis barrier (*57*, *58*). We further investigated the morphology of hydrogel-treated blood clot by cryo-SEM. The platelets and red blood cells were observed

within the mesh of hydrogel (fig. S17). This result suggested that the rapid blood clotting effect of the hydrogel in vitro may be related to the encapsulation and aggregation of platelets and red blood cells within the hydrogel networks.

Encouraged by its robust tissue adhesion and blood clotting effect, the 7% (w/v) HA-PEG hydrogel was evaluated as a potential sealant in a rat model of hepatic hemorrhage as well as in rabbit models of the femoral vein and artery bleeding to realize hemostasis. A rat model of hepatic hemorrhage was established by intraperitoneal injection of heparin, followed by partial excision of the left lobe of the liver. The precursor solution was applied to the wound to form a hydrogel in situ, when the liver was actively bleeding. To assess the hemostatic efficacy, the time to hemostasis was recorded. No hemostasis was observed within 10 min for heparinized rats in the control group. The hydrogel displayed robust adhesion on liver wounds and achieved hemostatic sealing of bleeding liver within 10 s, showing a significantly reduced time to hemostasis compared to the fibrin glue group (134 ± 43 s) (fig. S18). Furthermore, the blood loss within 3 min was recorded for each group. The hydrogel rapidly sealed off the tissue defect site, leading to a reduction of blood loss by 92.5% compared to the untreated group (Fig. 3G). To further evaluate the potential of the hydrogel for rapid hemostasis, incisions of 3 mm were created in the rabbit femoral artery and vein. Hemostatic forceps were used to clamp the blood vessels, and hydrogel was applied to the incisions. After 30 s, the forceps were removed. The hydrogel effectively sealed the incisions of both the artery and vein and prevented bleeding within 30 s (Fig. 3H).

Performance of the HA-PEG hydrogel for wound closure in full-thickness skin incisions

To further investigate the potential of 7% (w/v) HA-PEG hydrogel for wound closure, a rat full-thickness skin incision model was used (male, incision length = 2 cm). The precursor solutions were mixed and applied to the incision, followed by finger clamping for 2 min (Fig. 4A). Surgical suture, commercially available fibrin glue, and cyanoacrylate glue (Histoacryl) were used for comparison. The HA-PEG hydrogel could effectively close the wounds within 2 min and retained wound closure even under the influence of external forces of dragging and twisting (fig. S19 and movie S1). Moreover, the HA-PEG hydrogel was able to resist the tensile force of the skin during the wound healing process for a period of 14 days (Fig. 4B). In contrast, fibrin glue showed relatively weak tissue adhesion, and cyanoacrylate glue was brittle and easily peeled off from the skin. Therefore, the groups treated with fibrin glue and cyanoacrylate glue showed failed wound closure.

Histological analysis of the repaired skin was further performed using hematoxylin and eosin (H&E) and immunohistochemical staining. As shown in Fig. 4C and fig. S20, treatment with HA-PEG hydrogel resulted in a significantly reduced wound area on day 7 after treatment compared to that observed in the untreated group and groups treated with fibrin glue and cyanoacrylate glue. In addition, HA-PEG hydrogel–treated wounds exhibited minimal inflammation in H&E staining images on days 7 and 14. In comparison, a scar was observed extending from the dermis to the subcutaneous muscle layer in the untreated and cyanoacrylate glue–treated groups. In addition, the dermis layer was damaged by cyanoacrylate glue on day 7 after the glue film sloughed off from the skin. The application of fibrin glue showed more efficient wound closure than that observed in the untreated and cyanoacrylate glue–treated groups. Nevertheless, a high number of stained inflammatory cells were observed at the incision sites on day 7 in the H&E images of the fibrin glue–treated group, suggesting a severe inflammatory response. Immunohistochemical staining for CD68 further demonstrated a high level of macrophage recruitment in the wound area of the fibrin glue–treated group on day 7 (Fig. 5, A and D). Thus, the results indicated that the HA-PEG hydrogel accelerated the wound healing process by reducing inflammation at the wound site.

Collagen fibers play an important role in restoring tissue structure and function during wound healing. Collagen deposition in wounds was evaluated by Masson′s trichrome staining. An increase in collagen deposition was observed in all groups from days 7 to 14. Notably, the collagen level of the untreated group on day 14 was much lower than that of the HA-PEG and suture-treated groups (Fig. 5, B and E).

The vessels formed in the wound area were stained by CD31 with red fluorescence and differentiated myofibroblasts were stained by α-smooth muscle actin (α-SMA) with green fluorescence. As shown in Fig. 5C and fig. S20, regular expression of CD31 and α-SMA was observed after treatment with the HA-PEG hydrogel. Overall, the histological assessments indicated that rapid wound closure with HA-PEG hydrogel could reduce the wound area, relieve inflammation, promote collagen deposition, and consequently facilitate wound healing.

On-demand biodegradation of hydrogel through the incorporation of disulfide bonds

On the basis of the results of in vitro biocompatibility, ex vivo tissue adhesion, and in vivo hemostasis and wound closure, the HA-PEG hydrogel could achieve rapid wound closure and hemostasis, promote wound healing, and relieve inflammation at the wound sites. Because the time for wound healing is tissue specific, the degradation rate of tissue adhesives should match the rate of tissue repair. Meanwhile, on-demand degradation of adhesives allows for personalized treatment (*19*, *59*–*62*). Encouraged by this concept, we further introduced a stimulus-cleavable linker, 3,3′-dithiobis(propionohydrazide) (DTPH) containing a disulfide bond (SS), into the HA-PEG hydrogel network (Fig. 6A). The disulfide bond can be easily cleaved by thiol-containing compounds, a ubiquitous biological process that is key to the maintenance of protein structure and intracellular redox potential (*63*, *64*). The synthesis of DTPH-modified HA (HA-DTPH) was performed according to a procedure similar to that of HA-ADH (figs. S1 and S21). The HA-SS-PEG hydrogel was then formed by mixing HA-DTPH with 4aPEG-OPA in PBS at a mass ratio of 1:1 using the same cross-linking mechanism as that of the HA-PEG hydrogel (fig. S22). The HA-SS-PEG hydrogel demonstrated comparable gelation time, mechanical properties, and tissue adhesion strength to the HA-PEG hydrogel and showed good biocompatibility in vitro (figs. S22 to S26).

To investigate the stimuli-responsive degradation behavior in vitro, the HA-SS-PEG hydrogel was incubated in different media, including blank PBS, PBS with hyaluronidase, PBS with glutathione (GSH), and a cell culture medium. As shown in Fig. 6B, the HA-SS-PEG hydrogel continuously swelled for up to 30 days in blank PBS, while it was degraded in 12 days in the presence of hyaluronidase (10 U/ml) due to the accelerated degradation of HA segments in the hydrogel. In addition, owing to the disulfide bonds in the

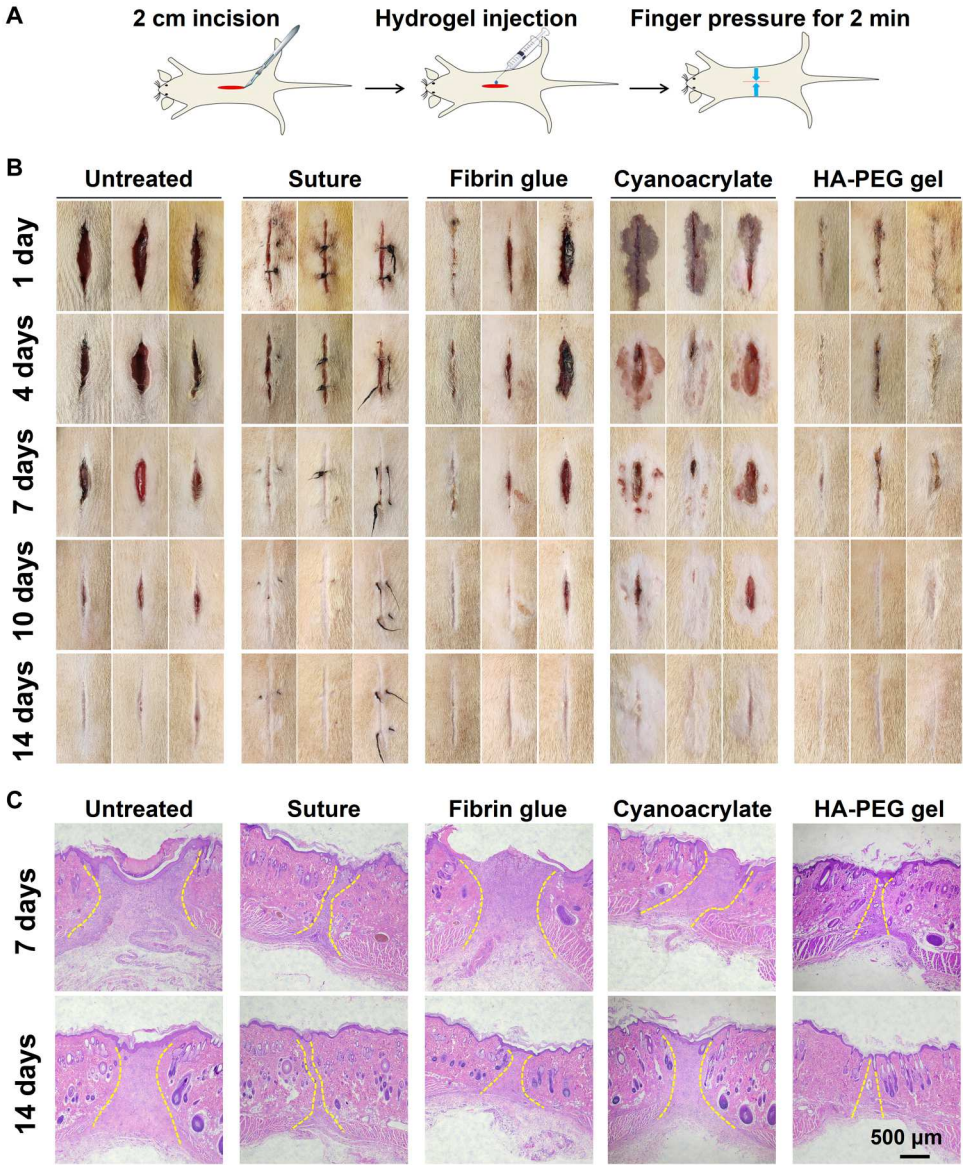

Fig. 4. Performance of HA-PEG hydrogel for wound closure in a rat full-thickness skin incision model. (**A**) Schematic illustration of the establishment and treatment of skin incision wounds by HA-PEG hydrogel or fibrin glue. (**B**) Representative photographs of wound areas after treatment with suture, fibrin glue, cyanoacrylate glue (Histoacryl), and 7% (w/v) HA-PEG hydrogel, respectively. (**C**) H&E staining images of wound tissues on days 7 and 14, respectively ($n = 3$). The yellow dashed lines indicate the remaining wound areas.

polymer network, the degradation rate could be adjusted by adding GSH (*65*). The HA-SS-PEG hydrogel was degraded within 2 days in the presence of 1 mM GSH. Increasing the GSH concentration to 5 mM led to a shorter degradation time of 1 day (Fig. 6C). Furthermore, to investigate the degradation behavior under more physiologically relevant conditions, we incubated the hydrogels in a cell culture medium. The HA-SS-PEG hydrogel could be degraded within 11 days in the cell culture medium, which was faster than the degradation rate of the HA-PEG hydrogel (19 days). Notably, the degradation time could be readily regulated by changing the HA-DTPH content in the hydrogel. By mixing HA-ADH, HA-DTPH, and 4aPEG-OPA at the mass ratio of 0.5:0.5:1, the resultant HA-ADH/HA-DTPH/4aPEG-OPA hydrogel, denoted as HA-$SS_{0.5}$-PEG, was degraded in 16 days (Fig. 6D and fig. S27). Therefore, the results demonstrated that the hydrogels exhibited tunable biodegradability.

Next, the hydrogels were subcutaneously implanted into rats for investigating their in vivo degradation behavior. The hydrogels demonstrated continuous biodegradation, as observed upon visual inspection and by noting changes in the weights of the remaining hydrogels (Fig. 6, E and F). The degradation rate of the HA-SS-PEG hydrogel (6 weeks) was much faster than that of HA-PEG (22 weeks), which was ascribed to the breakage of disulfide bonds in response to diverse thiol-containing compounds, for instance, GSH, found in vivo. The degradation rate of the hydrogels could also be regulated by adjusting the ratio of HA-DTPH in the

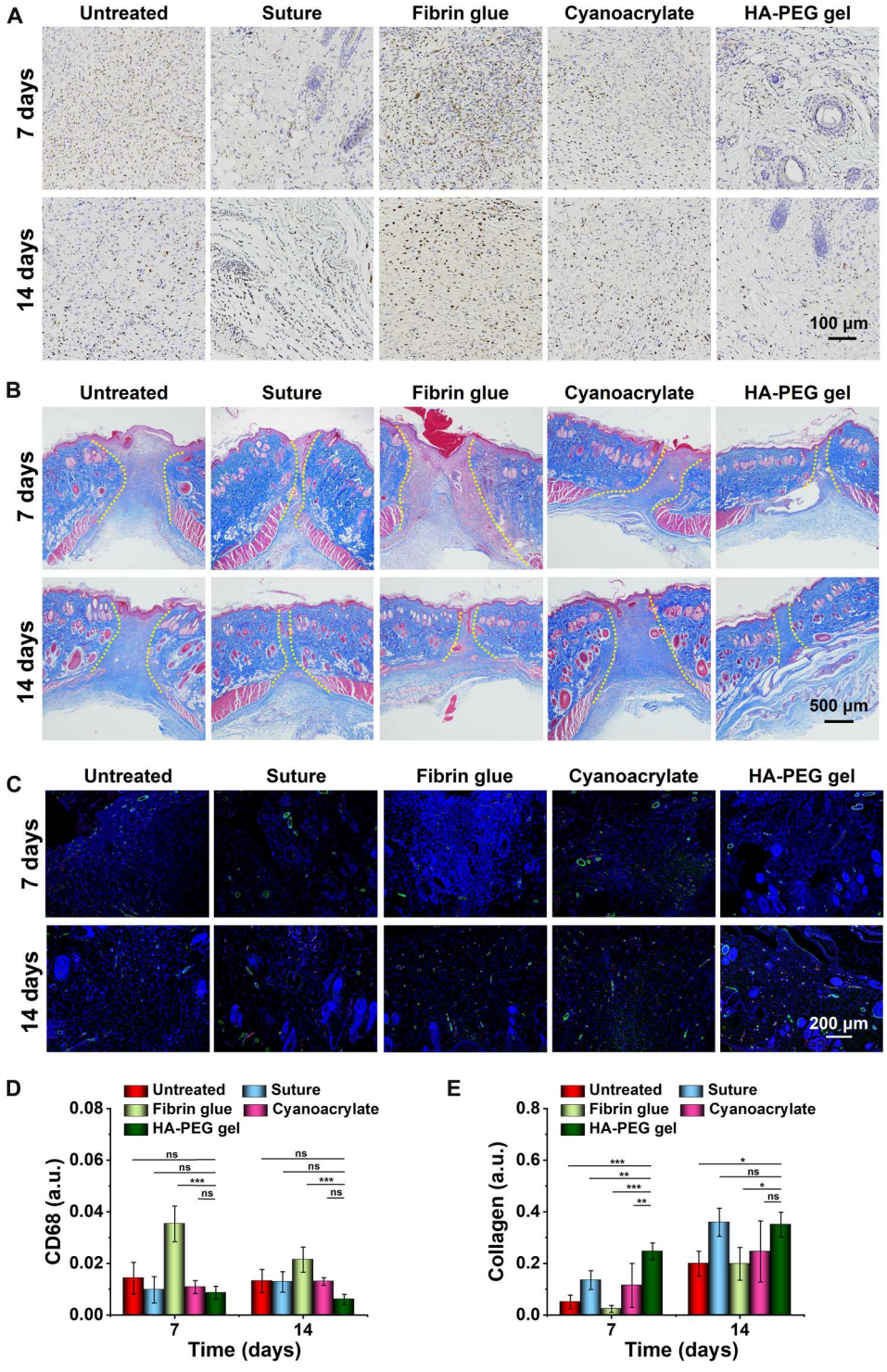

Fig. 5. Histological analysis of wound tissues. (**A**) Immunohistochemistry staining of macrophages (CD68), (**B**) Masson's trichrome staining, and (**C**) immunofluorescence staining of CD31 (red), α-SMA (green), and nuclei (blue) after treatments with suture, fibrin glue, cyanoacrylate glue, and 7% (w/v) HA-PEG hydrogel, respectively. The yellow dashed lines indicate the remaining wound areas in Masson's trichrome staining images. Quantification of (**D**) CD68 and (**E**) collagen at wound sites on days 7 and 14 after various treatments. a.u., arbitrary unit. Data are presented as mean ± SD ($n \geq 4$). Statistical significance was analyzed by two-way ANOVA with Tukey's post hoc test (*$P < 0.05$, **$P < 0.01$, and ***$P < 0.001$; ns, not significant).

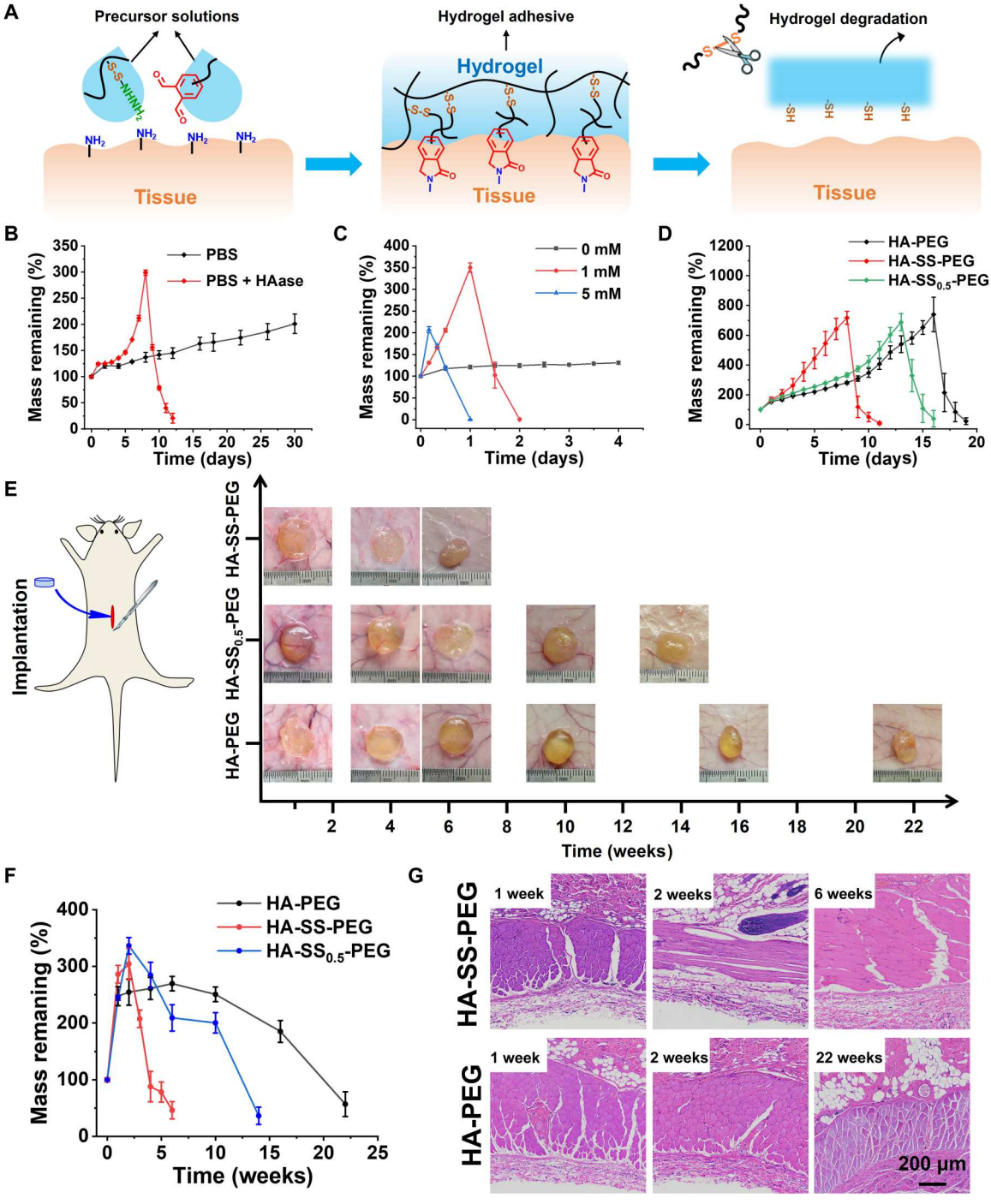

Fig. 6. On-demand hydrogel degradation through the incorporation of disulfide bonds. (**A**) Schematic illustration showing on-demand degradation of HA-SS-PEG hydrogel. (**B**) Degradation profiles of 7% (w/v) HA-SS-PEG hydrogel in blank PBS and PBS with hyaluronidase (10 U/ml) at 37°C (mean ± SD, $n = 3$). (**C**) Degradation profiles of 7% (w/v) HA-SS-PEG hydrogel in PBS with different concentrations of GSH at 37°C (mean ± SD, $n = 3$). (**D**) Degradation profiles of 7% (w/v) hydrogels with different contents of disulfide bonds in a cell culture medium at 37°C (mean ± SD, $n = 3$). (**E**) Representative images and (**F**) degradation profiles of 7% (w/v) hydrogels following subcutaneous implantation into rats at different time points (mean ± SD, $n = 3$). (**G**) H&E staining images for skin tissues surrounding different hydrogels at corresponding time points.

hydrogel. By mixing HA-ADH with HA-DTPH at equal mass ratio, the resultant HA-$SS_{0.5}$-PEG hydrogel was mostly degraded in 14 weeks. In addition, H&E staining showed enhanced accumulation of inflammatory cells at the tissue interfaces directly contacting the hydrogel 1 week after implantation, indicating mild inflammation caused by a normal foreign-body reaction (Fig. 6G and fig. S28) (*66*). It is notable that the inflammation was mitigated gradually as the hydrogels were degraded, implying good biocompatibility in vivo (*67*).

Performance of hydrogel for wound closure in rabbit full-thickness skin incisions

To evaluate the in vivo adhesion performance of the HA-PEG and HA-SS-PEG hydrogel, we established a rabbit full-thickness skin incision model (male, incision length, 3 cm) (Fig. 7A). The precursor polymer solutions were mixed and applied to the incisions. Suture, fibrin glue, and cyanoacrylate glue were used for comparison. As shown in Fig. 7B, both the HA-PEG and HA-SS-PEG hydrogel efficiently closed the wounds and resisted the tensile force of the skin for 20 days. The wounds treated with the HA-PEG or HA-SS-PEG hydrogel showed excellent healing efficiency, with negligible scars on day 20 after treatment. In contrast, the brittleness of cyanoacrylate glue and weak tissue adhesion of fibrin glue led to considerable failure of wound closure. It is worth noting that despite the effective wound closure observed upon treatment with sutures, scars associated with sutures were observed after wound healing.

We further histologically assessed the wound sites using H&E staining and Masson′s trichrome staining (Fig. 7C and fig. S29). The wound area was quantified on the basis of the H&E staining images to evaluate the wound healing effect. Treatment with HA-PEG or HA-SS-PEG hydrogel resulted in a significantly reduced wound area on day 10 after treatment compared to that observed in the untreated group and group treated with fibrin glue or cyanoacrylate glue (fig. S30A). The HA-PEG or HA-SS-PEG hydrogel–treated wounds exhibited reduced inflammation in H&E staining images on days 10 and 20. In addition, based on the Masson′s trichrome staining results, the collagen deposition levels at the wound sites of the HA-PEG and HA-SS-PEG hydrogel groups were significantly higher on day 10 after treatment, compared to that of the untreated group (fig. S30B). Notably, compared with the HA-PEG hydrogel, less residual hydrogel was found at the wound sites of the HA-SS-PEG hydrogel group based on H&E staining images (fig. S31). This was attributed to faster hydrogel degradation of the HA-SS-PEG hydrogel through the cleavage of disulfide bonds by diverse thiol compounds in vivo, for instance, GSH (*64*, *65*). It is worth mentioning that the timely degradation of hydrogel after the wound closure may be favorable for tissue regeneration and relieved inflammation (*68*). Overall, these results suggest that the HA-SS-PEG hydrogels exhibited excellent tissue adhesion, good biocompatibility, and controlled biodegradability and, hence, show promise as tissue adhesives for sutureless wound closure.

DISCUSSION

Sutures are the primary means to reconnect the injured tissues and close the wound areas after various injuries. However, suturing is a time-consuming process and may not be ideal in emergency situations. Besides, sutures will lead to additional damage to tissues and induce scarring. Tissue adhesives provide an attractive tool kit to rapidly close wounds, stop bleeding, prevent leakage, and ultimately restore tissue function.

Considerable commercially available and developing tissue adhesives use NHS ester/amine coupling reaction to form the cross-linking network and realize the tissue adhesion. They need to be used once upon dissolving in aqueous medium, owing to the hydrolytic instability of NHS ester (*32*). The limited operation time may compromise the performance of tissue adhesives. Tissue adhesives based on traditional Schiff base or hydrazone cross-linking strategy commonly exhibited low adhesion strength (*25*). In addition, the adhesives based on biomimetic polyphenol groups usually require the utilization of oxidants, which would compromise the biocompatibility of the system (*10*). A tissue adhesion mechanism based on transglutaminase-catalyzed conjugation between the glutamine groups of hydrogels and the amine groups in tissues was reported. The adhesion property of the hydrogels could be improved by incorporation of a second dynamic covalent cross-linking network (*69*).

HA hydrogel tissue adhesives based on traditional hydrazone bonds have been reported in several studies. However, these HA hydrogel adhesives showed weak tissue adhesion strength (1 to 3 kPa on porcine skin) (*70*). To improve the tissue adhesion properties of the HA hydrogel adhesives, polyphenol moieties were incorporated into the HA hydrogels, which led to additional hydrogel-tissue interactions including hydrogen bonding and covalent conjugation (*71*, *72*). With the presence of oxidation systems such as hydrogen peroxide and horseradish peroxidase, the tissue adhesion strengths of these hydrogels were increased to a certain extent (~13.8 kPa).

In this work, we developed an injectable and self-healing hydrogel adhesive with firm tissue adhesion and tunable degradation profile for wound closure and hemostatic sealing based on the catalyst-free OPA/amine (hydrazide) reaction. By simply mixing hydrazide-modified HA with 4aPEG-OPA, HA/PEG hybrid hydrogels were formed in situ through the formation of hydrazone linkages. Compared with preformed adhesives, the injectability of the hydrogel is favorable in certain circumstances, for example, minimally invasive procedures where access to the operative area is limited. The cross-linking process of HA/PEG hydrogels involved no initiator, catalyst, additive, or ultraviolet irradiation and yielded water as the only by-product. NMR spectroscopy and DFT calculation revealed that a cyclic IHBA intermediate was formed, arising from the double nucleophilic attack of a hydrazide group to the two adjacent aldehyde groups of OPA, which was then dehydrated to yield the hydrazone bond (*44*). The results explained the fast gelation process of HA/PEG hydrogels.

Owing to the fast and spontaneous coupling reaction between the residual OPA in the hydrogels and amine groups present in tissues, firm surface bonding formed between the HA/PEG hydrogels and tissues with the formation of stable phthalimidine linkages. In addition, the dynamic hydrazone cross-linking networks in the bulk hydrogels may contribute to the capability of energy dissipation. Thus, the HA/PEG hydrogel displayed firm adhesion to various tissues. The 7% (w/v) OPA/hydrazide cross-linked HA-PEG hydrogels exhibited a markedly enhanced adhesion strength (27.6 ± 3.9 kPa), compared to those of the 7% (w/v) benzaldehyde/hydrazide cross-linked hydrogel counterparts (0.9 ± 0.8 kPa) and a commercially available fibrin glue (12.1 ± 3.5 kPa).

Quick sealing and hemostasis of the bleeding wounds is crucial in clinical practice. In the in vitro blooding clotting tests, the HA-

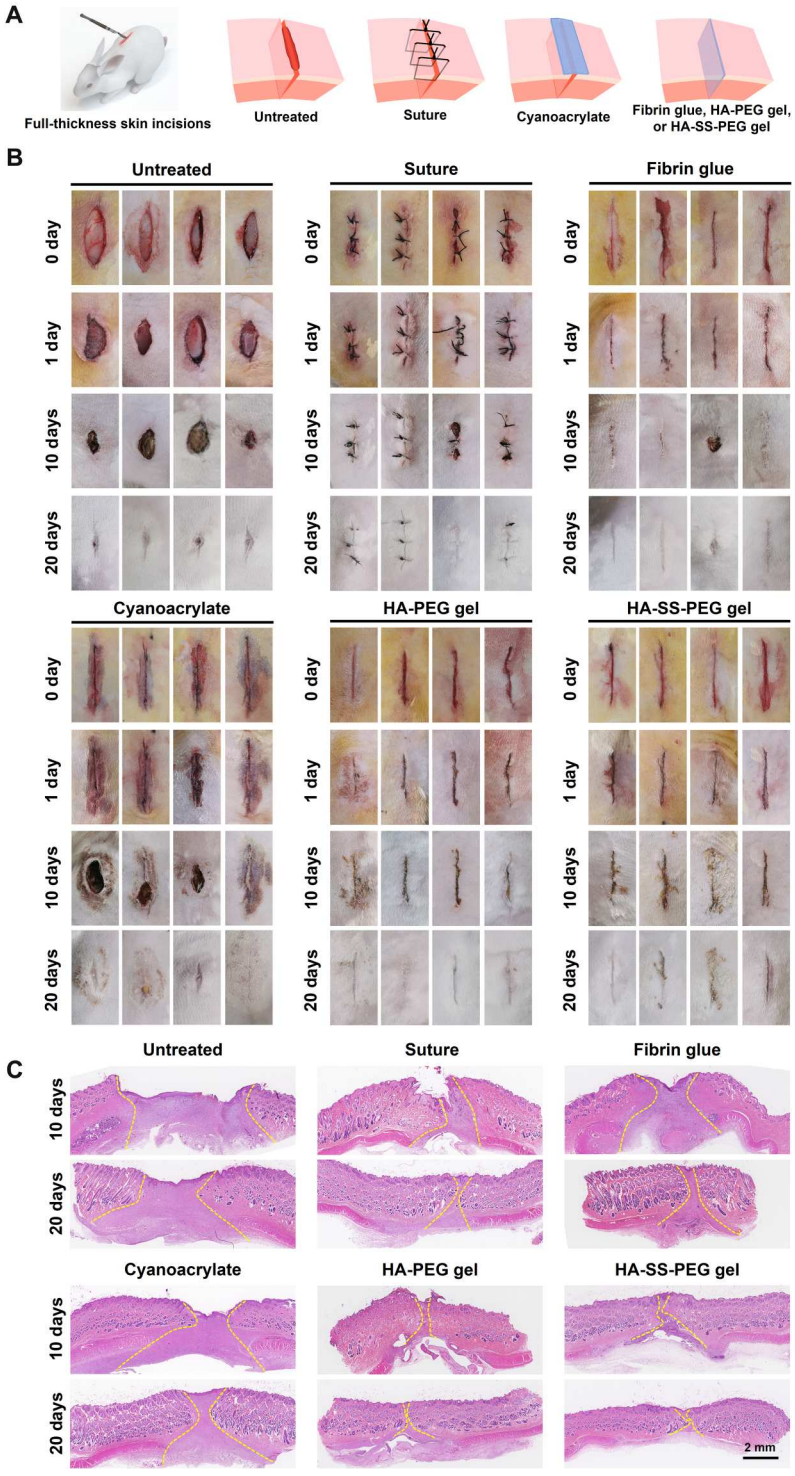

Fig. 7. Performance of hydrogel in wound closure in a rabbit full-thickness skin incision model. (**A**) Schematic illustration of the establishment and treatment of skin incision wounds. (**B**) Photographs of skin incision wounds after treatment with suture, fibrin glue, cyanoacrylate glue, 7% (w/v) HA-PEG hydrogel, and 7% (w/v) HA-SS-PEG hydrogel, respectively. (**C**) H&E staining of wound tissues on days 10 and 20, respectively (n = 4). The yellow dashed lines indicate the remaining wound areas.

PEG hydrogel was found to promote blood clotting, with encapsulation of platelets and red blood cells within the hydrogel. In animal models of liver and blood vessel bleeding, the hydrogels could effectively seal incisions and prevent bleeding rapidly. In rat and rabbit models of full-thickness skin incisions, the hydrogel adhesives could efficiently close the incisions within 2 min, withstand external forces of dragging and twisting, and ultimately promote wound healing with reduced inflammation and negligible scar formation. The hydrogels showed better performance in promoting wound closure and healing than commercially available fibrin glue and cyanoacrylate glue. Our results demonstrate that the OPA/amine (hydrazide) reaction can be adopted as a new adhesion chemistry for the development of tissue adhesives.

The biodegradation of adhesives at the desired rate circumvents the need for postoperative removal and prevents prolonged inflammation and tissue fibrosis caused by the foreign materials. The natural abundance of hyaluronidase is beneficial for the biodegradability of the HA/PEG hydrogel adhesives. The in vivo degradation profiles of hydrogels could be adjusted on demand by introducing disulfide bonds into the hydrogel network, which could be cleaved in response to diverse thiol-containing compounds, for instance, GSH, found in vivo. By adjusting the content of disulfide bonds in the hydrogel network, a wide range of degradation period (6 to 22 weeks) were obtained. This appealing property provides an opportunity to orchestrate the degradation rate of the adhesives according to the rate of tissue regeneration (*19*, *64*).

Biocompatibility is fundamental for clinical application of tissue adhesives. The two major components, HA and PEG, of the presented hydrogel adhesives are approved by FDA for clinical use. Our preliminary investigations demonstrated the good cytocompatibility and histocompatibility of the hydrogel adhesives. Future investigations are needed to evaluate the long-term degradation and metabolism in vivo. The studies on rat and rabbit models revealed the good performance of the hydrogel adhesives for hemostatic sealing and wound closure. Further evaluation and optimization of the performance on wound closure and tissue repair with large animal models are also important for the clinical translation of the material. Overall, the HA/PEG hydrogels with a biocompatible adhesion mechanism, superior tissue adhesion performance, and well-controlled biodegradation rate have shown strong potential for the development of next-generation tissue adhesives.

MATERIALS AND METHODS

Materials

HA (M_n = 35.0 kDa, polydispersity index = 2.5) was purchased from Bloomage Biotech Ltd. (Jinan, China). Hydrazine hydrate (40%) was purchased from Beijing Chemical Works (Beijing, China). Dimethyl 3,3′-dithiodipropionate (98%) and 1-hydroxybenzotriazole monohydrate (HOBt·H_2O) were obtained from Tokyo Chemical Industry Ltd. (Shanghai, China). Adipic acid dihydrazide, 1-(3-dimethylaminopropyl)-3-ethylcarbodiimide hydrochloride (EDC·HCl), and 4-formyl benzoic acid were purchased from J&K Scientific Ltd. (Beijing, China). Other reagents were purchased from the manufacturer and used without further purification. The 4aPEG (M_n = 10 kDa) was purchased from Pharmicell Co. Inc. (Seoul, Republic of Korea). Amino-terminated 4aPEG (M_n = 10 kDa) was obtained from JenKem Technology Co. Ltd. (Beijing, China). Cyanoacrylate glue (*n*-butyl-2-cyanoacrylate, Histoacryl) was obtained from B. Braun Surgical SA (Rubi, Spain). Fibrin glue derived from porcine plasma (Bioseal) was purchased from Bioseal Biotech Co. Ltd. (Guangzhou, China), a subsidiary company of Johnson & Johnson (New Jersey, USA).

Characterization

NMR spectra were recorded with a Bruker Avance III 500 MHz NMR spectrometer (Bruker, Germany) at 23°C using deuterium oxide (D_2O) or deuterated chloroform ($CDCl_3$) as the solvent. An MCR 301 rheometer (Anton Paar GmbH, Austria) with a flat upper plate (diameter, 25 mm) was used to determine the rheological behavior. Microstructures of hydrogels were investigated using a scanning electron microscope (Sigma 300, Zeiss, Germany). The tensile, compressive, and lap shear strengths of hydrogels were analyzed using a universal testing machine (AGS-X 50 N, SHIMADZU, Japan).

Synthesis of HA-ADH

HA-ADH was synthesized according to a previously reported procedure (*43*). First, HA (1.22 g, 3 mmol of disaccharide units) was dissolved in 200 ml of deionized water, and then, adipic acid dihydrazide (5.22 g, 30 mmol), HOBt·H_2O (405 mg, 3 mmol), and EDC·HCl (148 mg, 0.75 mmol) were successively added to the solution. Subsequently, the pH was adjusted to 4.7 using 1 M HCl and 1 M NaOH. The reaction was stirred for 48 hours at room temperature. The mixture was placed into a dialysis bag [molecular weight cutoff (MWCO): 7000 Da] and dialyzed against deionized water containing 0.9% (w/v) NaCl (6 × 2 liters) for 48 hours, followed by further dialysis against deionized water (3 × 2 liters) for 24 hours. HA-ADH was obtained after freeze drying, and the grafting rate was determined as 11.8% by ^{1}H NMR.

Synthesis of HA-DTPH

3,3′-Dithiobis(propanoic dihydrazide) was synthesized according to a previously reported procedure (*73*). Briefly, 3,3′-dithiopropionic acid dimethyl ester (10 g, 37.5 mmol) and hydrazine hydrate (12 g, 240 mmol) were dissolved in ethanol (20 ml). Then, the reaction was stirred and refluxed for 5 hours under a nitrogen atmosphere at 85°C. Subsequently, the mixture was washed with ice methanol (5 × 30 ml) and dried in vacuum. The product was recrystallized with ethanol-water at 60°C to obtain 3,3′-dithiobis(propanoic dihydrazide) (yield: 70.5%).

The synthesis method of HA-DTPH was similar to that of HA-ADH. HA (1.22 g, 3 mmol of disaccharide units) and 3,3′-dithiobis(propanoic dihydrazide) (6.24 g 30 mmol) were dissolved in 200 ml of deionized water. Subsequently, HOBt·H_2O (405 mg, 3 mmol) and EDC·HCl (178 mg 0.9 mmol) were added to the solution. The pH was adjusted to 4.7 using 1 M HCl and 1 M NaOH. The reaction was stirred at room temperature for 48 hours. The solution was placed into a dialysis bag (MWCO: 7000 Da) and dialyzed against deionized water containing 0.9% (w/v) NaCl (6 × 2 liters) for 48 hours, followed by further dialysis against deionized water (3 × 2 liters) for 24 hours. HA-DTPH was obtained after freeze drying, and the grafting rate was determined as 14.1% by ^{1}H NMR.

Synthesis of 4aPEG-OPA

1,3-Dimethoxy-1,3-dihydroisobenzofuran-5-carboxylic acid *N*-succinimidyl ester was synthesized according to our previously reported method (*36*). 4aPEG-OPA was synthesized as follows:

amino-terminated 4aPEG and 1,3-dimethoxy-1,3-dihydroisobenzofuran-5-carboxylic acid *N*-succinimidyl ester were dissolved in 20 ml of ultradry CH_2Cl_2, followed by the addition of 1 ml of pyridine. The yellow solid was precipitated with diethyl ether. Subsequently, the yellow solid was dissolved in deionized water, and trifluoroacetic acid was added. The mixture was stirred for 1 hour at room temperature and then dialyzed for 2 days to obtain 4aPEG-OPA. The degree of substitution of OPA was 75%, as determined by ^{1}H NMR.

Synthesis of 4aPEG-PhCHO

4aPEG (5 g, 2 mmol of hydroxyl groups) and 4-formyl benzoic acid (1.5 g, 10 mmol) were dissolved in 100 ml of CH_2Cl_2. Subsequently, EDC·HCl (3.8 g, 20 mmol) and 4-dimethylaminopyridine (0.24 g, 2 mmol) were added. The mixture was stirred at room temperature for 3 days. The solvent was evaporated in vacuum. The white solid was dissolved in deionized water, dialyzed against deionized water for 3 days, and eventually collected via lyophilization.

DFT calculations

All the geometry structures of reactants, intermediates, transition states, and products were optimized with the B3LYP method (*74*, *75*) and 6-31+G(d,p) basis set (*76*). The frequency analyses were performed at the same theoretical level. Frequencies of reactants, intermediates, and products are all positive values, while frequencies of transition states are only one negative value. Intrinsic reaction coordinate computation was carried out to check the reactant and product of each transition state (*77*). Solvent effect was also considered by computing single point energy with the M062x/6-311++G(d,p) method (*78*, *79*) and the SMD solvation model (*80*) on each optimized structure. All the computations were carried out with Gaussian 16 software. The three-dimensional molecule structures were drawn with CYLview.

Gelation time

The gelation time of hydrogel was determined by the tube inversion method. The precursor solutions in PBS with equivalent polymer concentrations were mixed at equal volume ratio, vortexed for 3 s, and then placed in a 37°C water bath. The formation of hydrogel was determined if no flow was observed after inverting the vial. The gelation time was recorded with three parallel tests.

Rheological test

Rheological tests were performed with a rheometer (MCR 301, Anton Paar GmbH, Austria) using parallel plates of 25 mm diameter with the gap fixed at 0.5 mm. The temperature of the lower plate was set at 37°C. Two precursor solutions with equivalent polymer concentrations were mixed at equal volume ratio, and the mixture was vortexed for 3 s, followed by immediately pipetting onto the bottom plate of the rheometer. For gelation kinetics measurements, the storage modulus (G') and loss modulus (G'') were recorded as a function of time at a frequency of 1 Hz and strain of 1%. A frequency sweep test was performed with frequencies ranging from 1 to 100 Hz with a constant strain of 1%. A strain sweep test was performed with strains ranging from 1 to 500% with a constant frequency of 1 Hz. The outer edge of the gap was sealed by a thin layer of silicone oil to prevent the evaporation of water. The self-healing properties of the hydrogels were measured by step-strain tests between a strain of 1 and 500% at 37°C with a constant frequency of 1 Hz.

Tensile and compression tests

Tensile and compressive tests were performed using a universal testing machine (AGS-X 50 N, SHIMADZU, Japan). For tensile tests, hydrogels were prepared in rectangular molds (5 mm by 2 mm by 12 mm) and incubated at 25°C for 6 hours before testing. The tensile rate was 2 mm/min. The tensile stress was calculated via dividing the load by the initial cross-sectional area. For compressive tests, hydrogels were prepared in cylindrical molds (diameter of 10 mm, height of 5 mm). The compressive rate was 1 mm/min. The compressive stress was obtained by dividing the load by the initial cross-sectional area. Each test was repeated at least three times. For cyclic compressive tests, cylindrical hydrogels (diameter of 10 mm, height of 5 mm) were cyclically compressed to a strain of 50% and returned to the initial height.

In vitro degradation behavior of hydrogels

Hydrogels (100 μl) were prepared in a small dish at room temperature. After 4 hours, 3 ml of the degradation medium [blank PBS, PBS with hyaluronidase (10 U/ml), Dulbecco's modified Eagle medium (DMEM) with 0.02% (w/v) NaN_3, PBS with 1 mM GSH, or PBS with 5 mM GSH] was added. At different time points, the medium was removed, and the weight of the hydrogel was measured. Three parallel samples were analyzed in each group.

In vitro cytocompatibility of materials

Mouse embryonic fibroblast cells (NIH 3T3) were cultured in DMEM containing 10% fetal bovine serum (Hyclone, Perbio Scientific, Sweden), penicillin (50 U/ml), and streptomycin (50 μg/ml) (Sigma-Aldrich). To evaluate the cytotoxicity of the polymers, NIH 3T3 cells were seeded in 96-well plates with 6000 cells per well. After incubation at 37°C for 24 hours, the medium was replaced with 200 μl of culture medium containing different concentrations of HA-ADH, HA-DTPH, 4aPEG-OPA, or polyethyleneimine (PEI). After 24 hours of incubation, the medium was removed, and the cells were washed twice with PBS. Then, 200 μl of culture medium containing 20 μl of CCK-8 solution was added to each well, followed by incubation for 2 hours at 37°C. A microplate reader (Tecan Group Ltd., Switzerland) was used to measure the absorbance at 450 nm. The cells cultured in the medium with PBS were used as the control. Cell viability is calculated as a percentage relative to the absorbance of the control group. Five parallel samples were analyzed in each group.

To evaluate the cytocompatibility of hydrogels, 25 μl of the 7% (w/v) HA-PEG or HA-SS-PEG hydrogel or PBS was added into a 48-well plate. Then, 1 ml of culture medium with 2×10^4 cells was added. After 24, 48, or 72 hours, the culture medium was replaced with 1 ml of fresh culture medium containing 100 μl of CCK-8 solution. After incubation for 2 hours at 37°C, the absorbance value was recorded at 450 nm using a microplate reader. Meanwhile, the cells were stained with Alexa Fluor 488 phalloidin and 4′,6-diamidino-2-phenylindole according to the manufacturer's protocol and observed with a confocal laser scanning microscope (CLSM) (CLSM 700, Carl Zeiss AG, Germany).

The survival of cells encapsulated within the hydrogel was assessed by live-dead staining. A mixture of 7% (w/v) precursor solution and cell suspension (2×10^4 cells/ml) was added to the glass-bottom plate. After cross-linking, 2 ml of culture medium was added to each dish. After 12 hours of culture, the cells were gently washed twice and incubated in PBS containing 2 μM

calcein acetoxymethyl ester and 4.5 μM propidium iodide for 2.5 hours. The cells were then imaged using CLSM.

In vitro hemolytic tests of materials

In vitro blood compatibility of hydrogel was performed according to previously reported protocols. Briefly, red blood cells were collected from the whole-blood samples of the rabbit by repeating centrifugation and washing (five times) and then diluted to 2% (v/v) with normal saline. The hydrogel extract was obtained by soaking the 7% (w/v) HA-PEG hydrogel in normal saline (200 mg/ml) for 24 hours. The extract (100%) and a series of twofold dilutions of the extract (50, 25, and 12.5%) were mixed with the erythrocyte suspension at the volume ratio of 1:1 and incubated for 2 hours at 37°C. Normal saline and deionized water were added instead of hydrogel extract as negative and positive controls, respectively. The mixture was centrifuged at 1500 rpm for 15 min, and the supernatant (200 μl) was transferred to a 96-well plate. The absorbance of the supernatant was measured at 540 nm using a microplate reader. Hemolysis ratio (%) was calculated as hemolysis ratio (%) = $(A_{sample} - A_{negative})/(A_{positive} - A_{negative}) \times 100\%$, where A represents the absorbance at 540 nm. Five parallel samples were used for each group.

In vitro adhesion properties

The lap shear test was performed using a universal testing machine (AGS-X 50 N, SHIMADZU, Japan) to evaluate the adhesion properties of HA-PEG and HA-SS-PEG hydrogels. Porcine skin was used as the adhesive matrix, and commercially available fibrin glue was used as the control. The porcine skin was first fixed on the glass using an industrial adhesive (ethyl cyanoacrylate, Tonglin Adhesives, Harbin, China), and the moisture was retained by placing it in a water bath at 37°C. Then, the HA-PEG hydrogel, HA-SS-PEG hydrogel, or fibrin glue was applied to the overlapping area of the two pieces of porcine skin (25 mm by 20 mm), after which a force of 2 N was applied for 2 hours at 37°C under humid conditions. The adhesion strengths were evaluated using the universal testing machine at the speed of 2 mm/min.

Next, a piece of 2.5 cm by 7.5 cm porcine skin was cut and cleaned with PBS. Then, 200 μl of 7% (w/v) HA-PEG hydrogel was injected onto the porcine skin at 25°C. After 30 min, stresses induced by stretch, bend, twist, and water flushing were applied on the HA-PEG hydrogel to examine the adhesion properties on the skin. Rhodamine B was added to the hydrogel for visualization.

In vitro adhesion of HA-PEG hydrogel to biological tissues, including the liver, kidney, and heart ex vivo, was also tested. They were soaked in PBS to retain moisture before use. After making an incision with a scalpel, an appropriate amount of 7% (w/v) HA-PEG hydrogel was injected into the incision, followed by clamping using fingers for 2 min. Photographs were captured after 20 min.

In vitro burst pressure

A burst pressure test was carried out to evaluate the sealing effect of the hydrogels. The porcine casings were soaked in PBS to retain moisture and cut into sheets of 3 cm by 3 cm. The casings were fixed on a home-designed burst pressure test device, and a 1.6 mm–diameter hole was created with a syringe. Then, 70 μl of HA-PEG hydrogel or fibrin glue was added to seal the hole. Ten minutes after sealing, the burst pressure was measured by pumping PBS (0.8 ml/min). Five parallel samples were used for each group.

In vivo degradation and biocompatibility

Animal experiments with rat models were performed according to the guidelines for the ethical review of laboratory animal welfare China National Standard (GB/T 35892-2018) and regulations on the administration of laboratory animals of China and approved by the Animal Ethics Committee of Changchun Institute of Applied Chemistry, Chinese Academy of Sciences (no. 2020-010). Male Sprague-Dawley rats (~7 weeks old, average body weight ~200 g) were purchased from Liaoning Changsheng Biotechnology Co. Ltd. (Benxi, Liaoning) and used for in vivo degradation. The rats were anesthetized by intraperitoneal injection of pentobarbital sodium (40 mg/kg). Incisions in the mediodorsal skin of rats were made, and lateral subcutaneous pockets were prepared. Hydrogel disks [7% (w/v), 150 μl] were prepared by mixing the hydrazide-modified HA and 4aPEG-OPA at a mass ratio of 1:1, followed by incubation at 37°C for 30 min. The hydrogel disks were then implanted into the rats under sterile conditions. At designated time points, the rats were euthanized. The remaining hydrogels were weighed, and the skins were processed for H&E staining.

In vitro blood clotting assay

The citrated whole blood was collected from healthy rabbits and mixed with 0.2 M calcium chloride solution at a 5:1 volume ratio by vortex for 3 s before use. Fifty microliters of hydrogel was placed in the bottom of 96-well plates, and 50 μl of blood sample was added. Fifty microliters of PBS and fibrin glue was used for comparison. At predetermined time points, the uncoagulated blood was gently removed by washing with PBS. The time to form a blood clot was recorded as the blood clotting time. The morphology of hydrogel-treated blood clot was investigated by using cryo-SEM.

Liver hemostasis

For the rat liver incision model, male Sprague-Dawley rats (6 to 8 weeks old, 180 to 200 g) were purchased from Liaoning Changsheng Biotechnology Co. Ltd. (Benxi, Liaoning) and randomly divided into three groups ($n = 5$ for each group). First, the rats were anticoagulated by intraperitoneal injection of heparin (3000 U/kg) 30 min before the operation. The animals were anesthetized with pentobarbital sodium and fixed on the operating board. The livers of the rats were exposed via an abdominal incision. The livers were partially excised at a point located 1 cm distally to the liver border. The fibrin glue or 7% (w/v) HA-PEG hydrogel was applied when the liver was actively bleeding. No treatment was performed in the control group. The time to hemostasis was recorded. The rats were euthanized to reduce animal pain if no hemostasis was observed within 10 min. In a separate experiment, the blood was collected with filter paper within 3 min after operation. Then, the filter paper was weighed, and the blood loss was calculated.

Vascular hemostasis

The femoral vein and femoral artery of male Japanese white rabbits (15 to 17 weeks old, ~2.5 kg) were used as vascular bleeding models. For femoral vein hemostasis, an incision (3 mm) was made with a scalpel. Hemostatic forceps were used to clamp the vein, and the 7% (w/v) HA-PEG hydrogel was applied at the incision site. After 30 s,

the forceps were withdrawn to examine whether the bleeding was stopped or not. The arterial hemostasis was performed using a similar method. An incision (3 mm) was made with a scalpel, and the hemostatic effect was observed 30 s after the application of the hydrogel.

Skin wound closure in the rat model

Male Sprague-Dawley rats (6 to 8 weeks old, ~210 g) were purchased from Liaoning Changsheng Biotechnology Co. Ltd. (Benxi, Liaoning) and used to demonstrate the application of HA-PEG hydrogels for wound closure. After anesthetization with pentobarbital sodium, the back of the rats was shaved and disinfected with povidone-iodine. A full-thickness skin incision of 2 cm was made on the dorsal midline of each rat with a scalpel. The 7% (w/v) HA-PEG hydrogel was administrated into the incisions, followed by finger clamping for 2 min. For comparison, fibrin glue was applied to the incisions, followed by finger clamping for 2 min. Cyanoacrylate glue (*n*-butyl-2-cyanoacrylate, Histoacryl) was applied on the surface of wounds to form a polymer film according to the manufacturer's protocol. A conventional suture was also applied for comparison. The rats were euthanized 7 and 14 days after the operation. The skin around the wounds was collected for histological assessments and immunohistochemical staining. Three animals were used for each treatment at each time point. Histological images were obtained with an inverted fluorescent microscope or CLSM. The wound area and collagen deposition level were analyzed on the basis of H&E and Masson's trichrome staining images, respectively, using the ImageJ software. The intensity of CD68 (marker of macrophages) and the immunofluorescence intensity of CD31 and α-SMA (marker of blood vessels) were quantified using the ImageJ software.

Skin wound closure in the rabbit model

Animal experiments with rabbit models were performed according to the Guidelines for the ethical review of laboratory animal welfare China National Standard (GB/T 35892-2018) and regulations on the administration of laboratory animals of China and approved by the Animal Ethics Committee of College of Basic Medical Sciences, Jilin University (nos. 2022-160 and 2023-218). Male Japanese white rabbits (15 to 17 weeks old, 2 to 2.5 kg) were purchased from Changchun Yisi Experimental Animals Technology Ltd. (Changchun, China) and used to evaluate the wound closure capacity of the HA-PEG or HA-SS-PEG hydrogel. After anesthetization with pentobarbital sodium, the back of the rabbits was shaved and sterilized with povidone-iodine. Four wounds (3 cm) were made on the back of each rabbit with a scalpel. The 7% (w/v) HA-PEG hydrogel, 7% (w/v) HA-SS-PEG hydrogel, or fibrin glue was applied to the incisions, followed by finger clamping for 2 min. Cyanoacrylate glue (*n*-butyl-2-cyanoacrylate, Histoacryl) was applied on the surface of wounds to form a polymer film according to the manufacturer's protocol. A conventional suture was also used for comparison. The rabbits were euthanized 10 and 20 days after the operation, and the skin around the wounds was collected for H&E and Masson's trichrome staining. The wound area and collagen deposition level were analyzed on the basis of H&E and Masson's trichrome staining images, respectively, using the ImageJ software. Four parallel samples were used for each group at each time point.

Statistical analysis

Experimental data are presented as means ± SD, and all experiments were conducted with at least three parallel samples. Statistical significance of all comparison results obtained in this study was determined using IBM SPSS statistics version 25 by performing an independent sample *t* test for two-group comparisons and one-way or two-way analysis of variance (ANOVA) for multiple-group comparisons, with Tukey's post hoc test ($^{*}P < 0.05$, $^{**}P < 0.01$, and $^{***}P < 0.001$).

Supplementary Materials

This PDF file includes:
Figs. S1 to S31
Legend for movie S1
Data S1

Other Supplementary Material for this manuscript includes the following:
Movie S1

REFERENCES AND NOTES

1. G. M. Taboada, K. Yang, M. J. N. Pereira, S. S. Liu, Y. Hu, J. M. Karp, N. Artzi, Y. Lee, Overcoming the translational barriers of tissue adhesives. *Nat. Rev. Mater.* **5**, 310–329 (2020).
2. S. Nam, D. Mooney, Polymeric tissue adhesives. *Chem. Rev.* **121**, 11336–11384 (2021).
3. G. R. Cosgrove, J. B. Delashaw, J. A. Grotenhuis, J. M. Tew, H. van Loveren, R. F. Spetzler, T. Payner, G. Rosseau, M. E. Shaffrey, L. N. Hopkins, R. Byrne, A. Norbash, Safety and efficacy of a novel polyethylene glycol hydrogel sealant for watertight dural repair. *J. Neurosurg.* **106**, 52–58 (2007).
4. K. S. Vyas, S. P. Saha, Comparison of hemostatic agents used in vascular surgery. *Expert Opin. Biol. Ther.* **13**, 1663–1672 (2013).
5. N. Annabi, K. Yue, A. Tamayol, A. Khademhosseini, Elastic sealants for surgical applications. *Eur. J. Pharm. Biopharm.* **95**, 27–39 (2015).
6. J. Li, A. D. Celiz, J. Yang, Q. Yang, I. Wamala, W. Whyte, B. R. Seo, N. V. Vasilyev, J. J. Vlassak, Z. Suo, D. J. Mooney, Tough adhesives for diverse wet surfaces. *Science* **357**, 378–381 (2017).
7. H. Yuk, C. E. Varela, C. S. Nabzdyk, X. Mao, R. F. Padera, E. T. Roche, X. Zhao, Dry double-sided tape for adhesion of wet tissues and devices. *Nature* **575**, 169–174 (2019).
8. A. Chow, H. Marshall, E. Zacharakis, P. Paraskeva, S. Purkayastha, Use of tissue glue for surgical incision closure: A systematic review and meta-analysis of randomized controlled trials. *J. Am. Coll. Surg.* **211**, 114–125 (2010).
9. A. P. Duarte, J. F. Coelho, J. C. Bordado, M. T. Cidade, M. H. Gil, Surgical adhesives: Systematic review of the main types and development forecast. *Prog. Polym. Sci.* **37**, 1031–1050 (2012).
10. P. J. M. Bouten, M. Zonjee, J. Bender, S. T. K. Yauw, H. van Goor, J. C. M. van Hest, R. Hoogenboom, The chemistry of tissue adhesive materials. *Prog. Polym. Sci.* **39**, 1375–1405 (2014).
11. C. Ghobril, M. W. Grinstaff, The chemistry and engineering of polymeric hydrogel adhesives for wound closure: A tutorial. *Chem. Soc. Rev.* **44**, 1820–1835 (2015).
12. W. D. Spotnitz, Fibrin sealant: Past, present, and future: A brief review. *World J.Surg.* **34**, 632–634 (2010).
13. A. J. Singer, J. V. Quinn, J. E. Hollander, The cyanoacrylate topical skin adhesives. *Am. J. Emerg. Med.* **26**, 490–496 (2008).
14. P. A. Leggat, D. R. Smith, U. Kedjarune, Surgical applications of cyanoacrylate adhesives: A review of toxicity. *ANZ J. Surg.* **77**, 209–213 (2007).
15. Y. Shi, D. Li, J. Ding, C. He, X. Chen, Physiologically relevant pH- and temperature-responsive polypeptide hydrogels with adhesive properties. *Polym. Chem.* **12**, 2832–2839 (2021).
16. H. Fan, J. Wang, J. P. Gong, Barnacle cement proteins-inspired tough hydrogels with robust, long-lasting, and repeatable underwater adhesion. *Adv. Funct. Mater.* **31**, 2009334 (2021).
17. J. Chen, D. Wang, L.-H. Wang, W. Liu, A. Chiu, K. Shariati, Q. Liu, X. Wang, Z. Zhong, J. Webb, R. E. Schwartz, N. Bouklas, M. Ma, An adhesive hydrogel with "load-sharing" effect as tissue bandages for drug and cell delivery. *Adv. Mater.* **32**, 2001628 (2020).

18. Y. Bu, L. Zhang, G. Sun, F. Sun, J. Liu, F. Yang, P. Tang, D. Wu, Tetra-PEG based hydrogel sealants for in vivo visceral hemostasis. *Adv. Mater.* **31**, 1901580 (2019).
19. X. Chen, H. Yuk, J. Wu, C. S. Nabzdyk, X. Zhao, Instant tough bioadhesive with triggerable benign detachment. *Proc. Natl. Acad. Sci. U.S.A.* **117**, 15497–15503 (2020).
20. B. R. Freedman, A. Kuttler, N. Beckmann, S. Nam, D. Kent, M. Schuleit, F. Ramazani, N. Accart, A. Rock, J. Li, M. Kurz, A. Fisch, T. Ullrich, M. W. Hast, Y. Tinguely, E. Weber, D. J. Mooney, Enhanced tendon healing by a tough hydrogel with an adhesive side and high drug-loading capacity. *Nat. Biomed. Eng.* **6**, 1167–1179 (2022).
21. J. Hu, T. Wei, H. Zhao, M. Chen, Y. Tan, Z. Ji, Q. Jin, J. Shen, Y. Han, N. Yang, L. Chen, Z. Xiao, H. Zhang, Z. Liu, Q. Chen, Mechanically active adhesive and immune regulative dressings for wound closure. *Matter* **4**, 2985–3000 (2021).
22. S. O. Blacklow, J. Li, B. R. Freedman, M. Zeidi, C. Chen, D. J. Mooney, Bioinspired mechanically active adhesive dressings to accelerate wound closure. *Sci. Adv.* **5**, eaaw3963 (2019).
23. Y. Hong, F. Zhou, Y. Hua, X. Zhang, C. Ni, D. Pan, Y. Zhang, D. Jiang, L. Yang, Q. Lin, Y. Zou, D. Yu, D. E. Arnot, X. Zou, L. Zhu, S. Zhang, H. Ouyang, A strongly adhesive hemostatic hydrogel for the repair of arterial and heart bleeds. *Nat. Commun.* **10**, 2060 (2019).
24. W. Zhang, B. Bao, F. Jiang, Y. Zhang, R. Zhou, Y. Lu, S. Lin, Q. Lin, X. Jiang, L. Zhu, Promoting oral mucosal wound healing with a hydrogel adhesive based on a phototriggered S-nitrosylation coupling reaction. *Adv. Mater.* **33**, 2105667 (2021).
25. J. Qu, X. Zhao, Y. Liang, T. Zhang, P. X. Ma, B. Guo, Antibacterial adhesive injectable hydrogels with rapid self-healing, extensibility and compressibility as wound dressing for joints skin wound healing. *Biomaterials* **183**, 185–199 (2018).
26. W. Zhu, Y. Peck, J. Iqbal, D. A. Wang, A novel DOPA-albumin based tissue adhesive for internal medical applications. *Biomaterials* **147**, 99–115 (2017).
27. D. Gan, W. Xing, L. Jiang, J. Fang, C. Zhao, F. Ren, L. Fang, K. Wang, X. Lu, Plant-inspired adhesive and tough hydrogel based on Ag-lignin nanoparticles-triggered dynamic redox catechol chemistry. *Nat. Commun.* **10**, 1487 (2019).
28. X. Xu, X. Xia, K. Zhang, A. Rai, Z. Li, P. Zhao, K. Wei, L. Zou, B. Yang, W.-K. Wong, P. W.-Y. Chiu, L. Bian, Bioadhesive hydrogels demonstrating pH-independent and ultrafast gelation promote gastric ulcer healing in pigs. *Sci. Transl. Med.* **12**, eaba8014 (2020).
29. J. Shin, S. Choi, J. H. Kim, J. H. Cho, Y. Jin, S. Kim, S. Min, S. K. Kim, D. Choi, S. W. Cho, Tissue tapes—Phenolic hyaluronic acid hydrogel patches for off-the-shelf therapy. *Adv. Funct. Mater.* **29**, 1903863 (2019).
30. J. Saiz-Poseu, J. Mancebo-Aracil, F. Nador, F. Busque, D. Ruiz-Molina, The chemistry behind catechol-based adhesion. *Angew. Chem. Int. Edit.* **58**, 696–714 (2019).
31. J. Guo, W. Wang, J. Hu, D. Xie, E. Gerhard, M. Nisic, D. Shan, G. Qian, S. Zheng, J. Yang, Synthesis and characterization of anti-bacterial and anti-fungal citrate-based mussel-inspired bioadhesives. *Biomaterials* **85**, 204–217 (2016).
32. S. Burks, W. Spotnitz, Safety and usability of hemostats, sealants, and adhesives. *AORN J.* **100**, 160–176 (2014).
33. N. A. Peppas, J. Z. Hilt, A. Khademhosseini, R. Langer, Hydrogels in biology and medicine: From molecular principles to bionanotechnology. *Adv. Mater.* **18**, 1345–1360 (2006).
34. N. Annabi, A. Tamayol, J. A. Uquillas, M. Akbari, L. E. Bertassoni, C. Cha, G. Camci-Unal, M. R. Dokmeci, N. A. Peppas, A. Khademhosseini, 25th anniversary article: Rational design and applications of hydrogels in regenerative medicine. *Adv. Mater.* **26**, 85–124 (2014).
35. J. L. Guo, Y. S. Kim, V. Y. Xie, B. T. Smith, E. Watson, J. Lam, H. A. Pearce, P. S. Engel, A. G. Mikos, Modular, tissue-specific, and biodegradable hydrogel cross-linkers for tissue engineering. *Sci. Adv.* **5**, eaaw7396 (2019).
36. Z. Zhang, C. He, Y. Rong, H. Ren, T. Wang, Z. Zou, X. Chen, A fast and versatile cross-linking strategy via *o*-phthalaldehyde condensation for mechanically strengthened and functional hydrogels. *Natl. Sci. Rev.* **8**, nwaa128 (2021).
37. C. L. Tung, C. T. Wong, E. Y. Fung, X. Li, Traceless and chemoselective amine bioconjugation via phthalimidine formation in native protein modification. *Org. Lett.* **18**, 2600–2603 (2016).
38. Y. Ma, Z. Lv, T. Li, T. Tian, L. Lu, W. Liu, Z. Zhu, C. Yang, Design and synthesis of ortho-phthalaldehyde phosphoramidite for single-step, rapid, efficient and chemoselective coupling of DNA with proteins under physiological conditions. *Chem. Commun.* **54**, 9434–9437 (2018).
39. R. D. Price, S. Myers, I. M. Leigh, H. A. Navsaria, The role of hyaluronic acid in wound healing. *Am. J. Clin. Dermatol.* **6**, 393–402 (2005).
40. J. A. Burdick, G. D. Prestwich, Hyaluronic acid hydrogels for biomedical applications. *Adv. Mater.* **23**, H41–H56 (2011).
41. X. Xu, A. K. Jha, D. A. Harrington, M. C. Farach-Carson, X. Jia, Hyaluronic acid-based hydrogels: From a natural polysaccharide to complex networks. *Soft Matter* **8**, 3280–3294 (2012).
42. M. N. Collins, C. Birkinshaw, Hyaluronic acid based scaffolds for tissue engineering—A review. *Carbohydr. Polym.* **92**, 1262–1279 (2013).
43. B. Yang, J. Song, Y. Jiang, M. Li, J. Wei, J. Qin, W. Peng, F. L. Lasaosa, Y. He, H. Mao, J. Yang, Z. Gu, Injectable adhesive self-healing multicross-linked double-network hydrogel facilitates full-thickness skin wound healing. *ACS Appl. Mater. Interfaces* **12**, 57782–57797 (2020).
44. P. Schmidt, L. Zhou, K. Tishinov, K. Zimmermann, D. Gillingham, Dialdehydes lead to exceptionally fast bioconjugations at neutral pH by virtue of a cyclic intermediate. *Angew. Chem. Int. Edit.* **53**, 10928–10931 (2014).
45. G. M. Kavanagh, S. B. Ross-Murphy, Rheological characterisation of polymer gels. *Prog. Polym. Sci.* **23**, 533–562 (1998).
46. J. Lou, R. Stowers, S. Nam, Y. Xia, O. Chaudhuri, Stress relaxing hyaluronic acid-collagen hydrogels promote cell spreading, fiber remodeling, and focal adhesion formation in 3D cell culture. *Biomaterials* **154**, 213–222 (2018).
47. Z. Zhang, C. He, X. Chen, Hydrogels based on pH-responsive reversible carbon–nitrogen double-bond linkages for biomedical applications. *Mat. Chem. Front.* **2**, 1765–1778 (2018).
48. S. Uman, A. Dhand, J. A. Burdick, Recent advances in shear-thinning and self-healing hydrogels for biomedical applications. *J. Appl. Polym. Sci.* **137**, 48668 (2020).
49. H. Tan, D. Jin, X. Qu, H. Liu, X. Chen, M. Yin, C. Liu, A PEG-lysozyme hydrogel harvests multiple functions as a fit-to-shape tissue sealant for internal-use of body. *Biomaterials* **192**, 392–404 (2019).
50. J. Wan, B. Wu, Y. Pan, Novel one-step synthesis of 2-carbonyl/thiocarbonyl isoindolinones and mechanistic disclosure on the rearrangement reaction of *o*-phthalaldehyde with amide/thioamide analogs. *Tetrahedron* **63**, 9338–9344 (2007).
51. A. C. A. D'Hollander, N. J. Westwood, Assessment of the regioselectivity in the condensation reaction of unsymmetrical *o*-phthaldialdehydes with alanine. *Tetrahedron* **74**, 224–239 (2018).
52. A. Assmann, A. Vegh, M. Ghasemi-Rad, S. Bagherifard, G. Cheng, E. S. Sani, G. U. Ruiz-Esparza, I. Noshadi, A. D. Lassaletta, S. Gangadharan, A. Tamayol, A. Khademhosseini, N. Annabi, A highly adhesive and naturally derived sealant. *Biomaterials* **140**, 115–127 (2017).
53. N. Annabi, Y. N. Zhang, A. Assmann, E. S. Sani, G. Cheng, A. D. Lassaletta, A. Vegh, B. Dehghani, G. U. Ruiz-Esparza, X. C. Wang, S. Gangadharan, A. S. Weiss, A. Khademhosseini, Engineering a highly elastic human protein-based sealant for surgical applications. *Sci. Transl. Med.* **9, eaai7466**, (2017).
54. D. A. Hickman, C. L. Pawlowski, U. D. S. Sekhon, J. Marks, A. Sen Gupta, Biomaterials and advanced technologies for hemostatic management of bleeding. *Adv. Mater.* **30**, 1870269 (2018).
55. C. Cui, C. Fan, Y. Wu, M. Xiao, T. Wu, D. Zhang, X. Chen, B. Liu, Z. Xu, B. Qu, W. Liu, Water-triggered hyperbranched polymer universal adhesives: From strong underwater adhesion to rapid sealing hemostasis. *Adv. Mater.* **31**, 1905761 (2019).
56. Y. Guo, Y. Wang, X. Zhao, X. Li, Q. Wang, W. Zhong, K. Mequanint, R. Zhan, M. Xing, G. Luo, Snake extract-laden hemostatic bioadhesive gel cross-linked by visible light. *Sci. Adv.* **7**, eabf9635 (2021).
57. W. Yang, X. Kang, X. Gao, Y. Zhuang, C. Fan, H. Shen, Y. Chen, J. Dai, Biomimetic natural biopolymer-based wet-tissue adhesive for tough adhesion, seamless sealed, emergency/nonpressing hemostasis, and promoted wound healing. *Adv. Funct. Mater.* **33**, 2211340 (2023).
58. K. Kim, J. H. Ryu, M.-Y. Koh, S. P. Yun, S. Kim, J. P. Park, C.-W. Jung, M. S. Lee, H.-I. Seo, J. H. Kim, H. Lee, Coagulopathy-independent, bioinspired hemostatic materials: A full research story from preclinical models to a human clinical trial. *Sci. Adv.* **7**, eabc9992 (2021).
59. M. D. Konieczynska, M. W. Grinstaff, On-demand dissolution of chemically cross-linked hydrogels. *Acc. Chem. Res.* **50**, 151–160 (2017).
60. B. Xue, J. Gu, L. Li, W. Yu, S. Yin, M. Qin, Q. Jiang, W. Wang, Y. Cao, Hydrogel tapes for fault-tolerant strong wet adhesion. *Nat. Commun.* **12**, 7156 (2021).
61. H. Lu, L. Yuan, X. Yu, C. Wu, D. He, J. Deng, Recent advances of on-demand dissolution of hydrogel dressings. *Burns Trauma* **6**, 35 (2018).
62. Y. Gao, K. Wu, Z. Suo, Photodetachable adhesion. *Adv. Mater.* **31**, 1806948 (2019).
63. G. A. Barcan, X. Zhang, R. M. Waymouth, Structurally dynamic hydrogels derived from 1,2-dithiolanes. *J. Am. Chem. Soc.* **137**, 5650–5653 (2015).
64. J. R. Clegg, A. S. Irani, E. W. Ander, C. M. Ludolph, A. K. Venkataraman, J. X. Zhong, N. A. Peppas, Synthetic networks with tunable responsiveness, biodegradation, and molecular recognition for precision medicine applications. *Sci. Adv.* **5**, aax7946 (2019).
65. Q. Xu, C. He, Z. Zhang, K. Ren, X. Chen, Injectable, biomolecule-responsive polypeptide hydrogels for cell encapsulation and facile cell recovery through triggered degradation. *ACS Appl. Mater. Interfaces* **8**, 30692–30702 (2016).
66. O. Veiseh, A. J. Vegas, Domesticating the foreign body response: Recent advances and applications. *Adv. Drug Deliv. Rev.* **144**, 148–161 (2019).
67. K. Ren, C. He, C. Xiao, G. Li, X. Chen, Injectable glycopolypeptide hydrogels as biomimetic scaffolds for cartilage tissue engineering. *Biomaterials* **51**, 238–249 (2015).

68. A. K. Gaharwar, I. Singh, A. Khademhosseini, Engineered biomaterials for in situ tissue regeneration. *Nat. Rev. Mater.* **5**, 686–705 (2020).
69. J. Chen, J. S. Caserto, I. Ang, K. Shariati, J. Webb, B. Wang, X. Wang, N. Bouklas, M. Ma, An adhesive and resilient hydrogel for the sealing and treatment of gastric perforation. *Bioact. Mater.* **14**, 52–60 (2022).
70. Z. Li, F. Zhou, Z. Li, S. Lin, L. Chen, L. Liu, Y. Chen, Hydrogel cross-linked with dynamic covalent bonding and micellization for promoting burn wound healing. *ACS Appl. Mater. Interfaces* **10**, 25194–25202 (2018).
71. M. Li, Y. Liang, Y. Liang, G. Pan, B. Guo, Injectable stretchable self-healing dual dynamic network hydrogel as adhesive anti-oxidant wound dressing for photothermal clearance of bacteria and promoting wound healing of MRSA infected motion wounds. *Chem. Eng. J.* **427**, 132039 (2022).
72. S. Samanta, V. K. Rangasami, H. Sarlus, J. R. K. Samal, A. D. Evans, V. S. Parihar, O. P. Varghese, R. A. Harris, O. P. Oommen, Interpenetrating gallol functionalized tissue adhesive hyaluronic acid hydrogel polarizes macrophages to an immunosuppressive phenotype. *Acta Biomater.* **142**, 36–48 (2022).
73. N. Cui, J. Qian, W. Xu, M. Xu, N. Zhao, T. Liu, H. Wang, Preparation, characterization, and biocompatibility evaluation of poly(N_ε-acryloyl-L-lysine)/hyaluronic acid interpenetrating network hydrogels. *Carbohydr. Polym.* **136**, 1017–1026 (2016).
74. A. D. Becke, A new mixing of Hartree-Fock and local density-functional theories. *J. Chem. Phys.* **98**, 1372–1377 (1993).
75. C. T. Lee, W. T. Yang, R. G. Parr, Development of the Colle-Salvetti correlation-energy formula into a functional of the electron-density. *Phys. Rev. B* **37**, 785–789 (1988).
76. M. M. Francl, W. J. Pietro, W. J. Hehre, J. S. Binkley, M. S. Gordon, D. J. Defrees, J. A. Pople, Self-consistent molecular orbital methods. XXIII. A polarization-type basis set for second-row elements. *J. Chem. Phys.* **77**, 3654–3665 (1982).
77. K. Fukui, The path of chemical reactions–The IRC approach. *Acc. Chem. Res.* **14**, 363–368 (1981).
78. Y. Zhao, D. G. Truhlar, The M06 suite of density functionals for main group thermochemistry, thermochemical kinetics, noncovalent interactions, excited states, and transition elements: Two new functionals and systematic testing of four M06-class functionals and 12 other functionals. *Theor. Chem. Acc.* **120**, 215–241 (2008).
79. Y. Zhao, D. G. Truhlar, Density functionals with broad applicability in chemistry. *Acc. Chem. Res.* **41**, 157–167 (2008).
80. A. V. Marenich, C. J. Cramer, D. G. Truhlar, Universal solvation model based on solute electron density and on a continuum model of the solvent defined by the bulk dielectric constant and atomic surface tensions. *J. Phys. Chem. B* **113**, 6378–6396 (2009).

Acknowledgments

Funding: We are grateful for the financial support from the National Natural Science Foundation of China (projects 52173147, 22105198, 51973218, and 51833010) and the Scientific and Technological Development Projects of Jilin Province (20210204136YY). **Author contributions:** Conceptualization: H.R., Z. Zhang, X. Chen, and C.H. Methodology: H.R., Z. Zhang, X. Chen, and C.H. Investigation: H.R., Z. Zhang, X. Cheng, and Z. Zou. Visualization: H.R. Supervision: X. Chen and C.H. Writing—original draft: H.R. and Z. Zhang. Writing—review and editing: X. Chen and C.H. **Competing interests:** The authors declare that they have no competing interests. **Data and materials availability:** All data needed to evaluate the conclusions in the paper are present in the paper and/or the Supplementary Materials.

Submitted 3 March 2023
Accepted 14 July 2023
Published 16 August 2023
10.1126/sciadv.adh4327